CHAPTER 5

PROPOSAL FOR DESIGN OR VERIFICATION CRITERIA FOR BEAMS SUBJECTED TO TRANSVERSE LOADS

5.1. Introduction

In the case of a beam under transverse loads, the different laminate and interface stress distributions derived in Chapter 4 allow us to understand the behavior of an externally reinforced element not only between two cracks but also at the end of the laminate. However, the formulae are awkward for design purposes, because in addition to a moment-curvature analysis, it is necessary to solve many differential equations. There is a need to find a simple effective method to design the strengthening of an existing structure with an externally bonded plate but preventing the premature peeling failure that causes the laminate debonding. This chapter describes a new design or verification method based on a maximum shear force-bending moment relationship associated to the theoretical maximum transferred force between cracks before peeling occurs. The basis of the design criteria are described in §5.2. Details of the verification and design procedure are given in §5.3 and §5.4 respectively. An application example of the proposed method in the design of an externally bonded laminate to strengthen an existing structure is presented in §5.5. Finally, the proposal is verified by means of the assembled bending test database (see §5.6).

5.2. Basis of the design criteria

5.2.1. Introduction

The basis of the design criteria will be dealt with first. The structural element will safely support the external loads if at every section the resistance of the element exceeds the effect of the loads. Thus, the design value of the shear forces and bending moments related to load effects should be lower than both the ultimate bending moment and the ultimate shear force.

As mentioned in previous chapters, the main problems with structures externally strengthened by plate bonding are the brittle modes of failure that limit the significant enhancement derived from the use of composite materials. These brittle modes of failure involve the debonding of the external reinforcement. Debonding can initiate near flexural or shear cracks along the span, or at the laminate end. Even though both situations are critical for design or verification purposes, the bending test database has shown that peeling failure due to the effect of cracks is more common than peeling failure at the laminate end. Hence, a methodology to prevent peeling failure initiated near cracks will be developed at first. Once a prediction in terms of ultimate bending moment or ultimate shear force is obtained, the element between the laminate end and the nearest crack will be verified. If the laminate end verification results more critical, a readjustment of the previously derived prediction will be performed.

It is possible to find the maximum shear force acting between two cracks before peeling failure occurs by assuming that debonding starts when the transferred force between concrete and laminate reaches its maximum value.

For this purpose a beam element between two cracks, I and J, is studied (Figure 5.1). The crack distance between them is given as s_{cr}. It is assumed that the bending moment increases from crack I to crack J. By applying equilibrium to this element, equations (5.1) and (5.2) are derived.

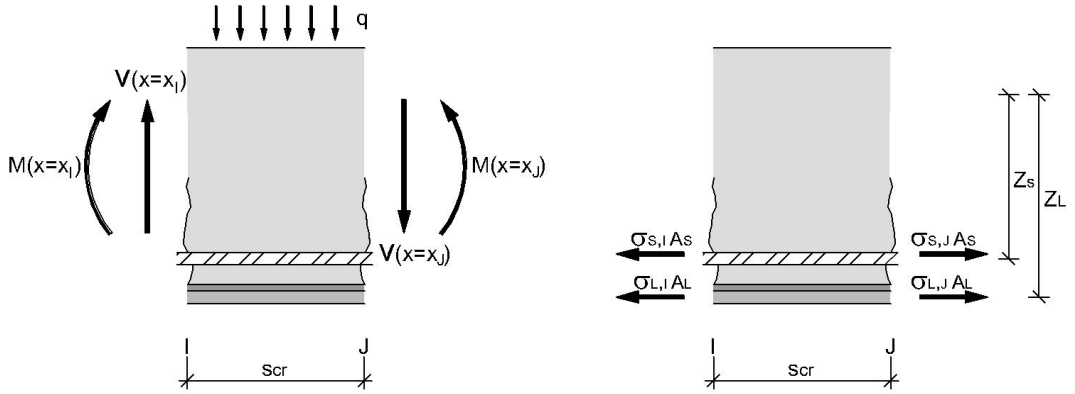

Figure 5.1. Crack element between crack I and J.

$$V_J = V_I - q\, s_{cr} \tag{5.1}$$

$$\Delta M_{IJ} = V_J\, s_{cr} + q\frac{s_{cr}^2}{2} \tag{5.2}$$

where:

V_J: shear force acting on crack J ($V(x = x_J)$)
ΔM_{IJ}: bending moment increment between crack I and crack J

From the sectional analysis of cracks I and J, the bending moment acting on those sections can be expressed as a function of the tensile stress in both the laminate and the internal reinforcement. The bending moment increment is given by equation (5.3).

$$\Delta M_{IJ} = \left(\sigma_{L,J} z_{L,J} - \sigma_{L,I} z_{L,I}\right) A_L + \left(\sigma_{s,J} z_{s,J} - \sigma_{s,I} z_{s,I}\right) A_s \tag{5.3}$$

where:

$\sigma_{L,I}$, $\sigma_{L,J}$: laminate tensile stress in cracks I and J respectively
$\sigma_{s,I}$, $\sigma_{s,J}$: longitudinal steel tensile stress in cracks I and J respectively
$z_{L,I}$, $z_{L,J}$: laminate lever arms in cracks I and J respectively
$z_{s,I}$, $z_{s,J}$: internal steel lever arms in cracks I and J respectively

Assuming that for both internal and external reinforcements the lever arms (z_L, z_s) of sections I and J are similar, equation (5.3) can be simplified as shown in equation (5.4). In addition, by incorporating equation (5.2) into (5.3), the bending moment increment can also be expressed as a function of the shear force on the J cross-section and the transverse load acting along the crack distance.

$$\Delta M_{IJ} = \Delta\sigma_{L,IJ} A_L z_L + \Delta\sigma_{s,IJ} A_s z_s = V_J \, s_{cr} + q \frac{s_{cr}^2}{2} \tag{5.4}$$

where:

$\Delta\sigma_{L,IJ}$: laminate tensile stress increment between cracks I and J
$\Delta\sigma_{s,IJ}$: longitudinal steel tensile stress increment between cracks I and J

Using equation (5.4), it can be inferred that the shear force acting on crack J has a limit value depending on the maximum force transferred by the laminate and the internal steel, as shown in equation (5.5).

$$V_{J,\max} = \frac{1}{s_{cr}} \left(\Delta\sigma_{L,IJ,\max} A_L z_L + \Delta\sigma_{s,IJ} A_s z_s\right) - q \frac{s_{cr}}{2} \tag{5.5}$$

The maximum transferred force between the external laminate and the support before debonding, $\Delta\sigma_{L,IJ,\max} A_L$ was given as $\Delta P_{\max,scr}$ in Chapter 4 for either short or long crack distances (see equations (4.75) or (4.79) of Chapter 4).

$$V_{J,\max} = \frac{1}{s_{cr}} \left(\Delta P_{\max,scr} z_L + \Delta\sigma_{s,IJ} A_s z_s\right) - q \frac{s_{cr}}{2} \tag{5.6}$$

As described in §4.3.6 of Chapter 4, the maximum transferred force for short crack distances is reached at the beginning of Stage 2b. In addition, for long crack distances,

the maximum transferred force is reached when Stage 3b initiates (see Figure 5.2). By substituting the maximum transferred force given by equations (4.75) or (4.79) into equation (5.6), the maximum shear force before a premature peeling failure occurs can be obtained for any crack distance.

Note that once the maximum transferred force between two cracks is reached, any attempt to increase the external applied load will result in brittle laminate debonding. The evolution of Stages 2b or 3b will only be possible when controlling the slip in both cracks I and J (which is almost impossible in a real case) and if the internal steel has not yielded in both cracks I and J (see Chapter 4).

As shown in Chapter 4, when the maximum transferred force is reached in a short crack distance, the shear stresses are transferred throughout the whole crack distance, s_{cr}. Thus, both the maximum transferred force and the maximum shear force are a function of s_{cr}. For long crack distances, the maximum transferred force is reached after a macrocrack has already appeared (at the beginning of Stage 3b). The shear stress transfer is only possible along the remaining bonded length, $L_b = s_{cr} - L_{mcrack}$, which is equal to the limit between a short and long crack distance, $s_{cr,\lim}$ (see Chapter 4). Hence, for long crack distances, both the maximum transferred force and the maximum shear force depend on the limit between a short and long crack distance, $s_{cr,\lim}$.

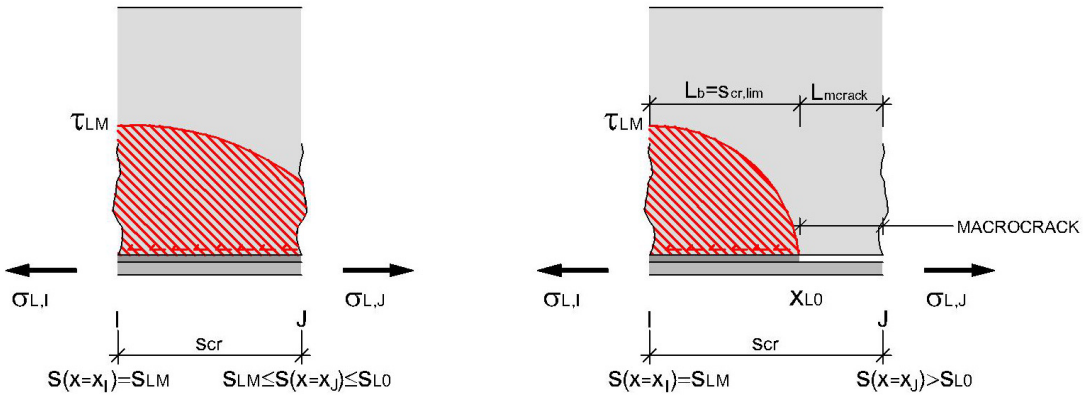

Figure 5.2. Maximum transferred force in short and long crack distances.

By incorporating equations (4.75) or (4.79) into equation (5.6), and neglecting the concrete's contribution in tension, the maximum shear force can be rewritten as a function of the theoretical transferred force of a pure shear specimen, whose length is the remaining bonded length L_b between cracks, and as a function of υ (see equation (4.42)) which relates the laminate tensile stress in both cracks I and J.

$$V_{J,\max} = \frac{1}{s_{cr}}\left(\frac{1-\upsilon}{1-\upsilon\cos(\Omega_2 L_b)}P_{\max,Lb}z_L + \Delta\sigma_{s,IJ}A_s z_s\right) + q\frac{s_{cr}}{2} \tag{5.7}$$

For short crack distances, the bonded length is equal to s_{cr}. For long crack distances, the remaining bonded length is equal to $s_{cr,\lim}$ given by equation (4.51). After incorporating equation (4.51) into equation (5.7), the more simplified equation (5.8) is obtained for long crack distances.

$$V_{J,\max} = \frac{1}{s_{cr}}\left(\frac{P_{\max,Lb} z_L}{1+\upsilon} + \Delta\sigma_{s,IJ} A_s z_s\right) + q\frac{s_{cr}}{2} \tag{5.8}$$

According to equation (5.6), the maximum shear force depends on the internal steel state in both cracks I and J, in other words, on the yielding of the internal steel. As shown in equation (5.7), the influence of steel yielding is shown not only by the internal steel transferred force but also by the laminate transferred force, which depends on the steel state through the υ function.

Depending on the bending moment acting on both cracks I and J, three possible cases can be distinguished.

Case 1: $M(x = x_J) < M_y$ (Internal steel reinforcement unyielded in either crack I or crack J)

Case 2: $M(x = x_J) \geq M_y$ and $M(x = x_I) < M_y$ (Internal steel reinforcement yielded in crack J but not in crack I)

Case 3: $M(x = x_J) \geq M_y$ and $M(x = x_I) \geq M_y$ (Internal steel reinforcement yielded in both cracks I and J)

As an alternative to equation (5.6), the same value for the maximum shear force can be obtained from the limit condition for the tensile stress of Stages 2b and 3b as given by equations (4.46) and (4.65), respectively.

5.2.2. Maximum shear force limit

As mentioned in the previous section, for each bending moment on crack J, it is possible to find the maximum allowable force acting on this crack before peeling occurs. The maximum shear force depends on the crack distance and the internal steel yielding.

This section describes the procedure to obtain the relationship between the bending moment acting on crack J and the maximum shear force that can be reached assuming maximum transmission of shear stresses along the interface. This relationship will be used later on for design or verification purposes.

First of all, the crack distance should be estimated. If the analyzed element was subjected to a certain load state that induced the formation of cracks prior to the application of the external reinforcement, the initial crack distance can be estimated as shown in the Spanish Concrete Code, EHE (1999). As the load increases above the service load, the crack distance is reduced by the formation of some intermediate cracks. Thus, the crack distance can be reduced by half. In case the beam was not preloaded before FRP bonding, the crack distance can be calculated by assuming a certain contribution of the externally bonded laminate to the crack formation. This is shown in the guidelines of the FIB Task Group 9.3 FRP (2001).

By performing a moment-curvature analysis of the strengthened section, the bending moment that causes steel yielding is obtained as M_y.

Once both the crack distance and the steel yield bending moment are known, the maximum shear force before peeling occurs can be obtained for any bending moment value on crack J. Three different cases will be distinguished depending on the internal steel state. For each case, a summary of the steps that should be followed to obtain the shear force limit is presented below. Note that the following formulae which has been derived for a general case can be simplified to a three-or-four point bending configuration by assuming $q = 0$.

Case 1: $M(x = x_J) < M_y$ and $M(x = x_I) < M_y$ (Internal steel reinforcement unyielded in either crack I or J)

First, the limit between a short and long crack distance, $s_{cr,\lim}$, is obtained for the maximum shear force by solving equation (5.9) for each bending moment acting on crack J lower than the yielding bending moment.

$$\begin{aligned}&\frac{\tau_{LM} b_L}{\Omega_2} z_L + \frac{2\kappa A_L z_L}{\Omega_2^2 s_{cr,\lim}^2} \sin\left(\Omega_2 s_{cr,\lim}\right) - \frac{\kappa A_L z_L}{\Omega_2 s_{cr,\lim}} \left(1 + \cos\left(\Omega_2 s_{cr,\lim}\right)\right) - \\ &- M\left(x = x_J\right)\left(1 - \frac{f_y A_s z_s}{M_y}\right) \sin\left(\Omega_2 s_{cr,\lim}\right) = 0\end{aligned} \tag{5.9}$$

where:

κ: constant given by equation (5.10)

$$\kappa = -\mu s_{cr,\lim}^2 = 4\beta f_{ctm} \frac{E_L}{E_C} \tag{5.10}$$

The maximum shear force before peeling occurs can be obtained as shown by equation (5.11) which is a function of the bending moment on crack J and of the laminate bonded length. Depending on the bonded length, the maximum shear force will be obtained at the beginning of Stage 2b (short crack distances) or at the beginning of Stage 3b (long crack distances).

$$\begin{aligned}V_{J,\max} = &\frac{1}{s_{cr} \cos\left(\Omega_2 L_b\right)\left(1 - \frac{f_y A_s z_s}{M_y}\right)} \left\{ P_{\max,L=Lb} z_L + \frac{2\kappa A_L z_L}{\Omega_2^2 s_{cr}^2}\left(1 - \cos\left(\Omega_2 L_b\right)\right) \right. \\ &\left. - \frac{\kappa A_L z_L}{\Omega_2 s_{cr}} \sin\left(\Omega_2 L_b\right) - M\left(x = x_J\right)\left(1 - \frac{f_y A_s z_s}{M_y}\right)\left(1 - \cos\left(\Omega_2 L_b\right)\right) \right\} - q\frac{s_{cr}}{2}\end{aligned} \tag{5.11}$$

where:

L_b: bonded length calculated as the minimum value between the estimated crack distance and the limit between a short and long crack distance

- for short crack distances ($s_{cr} < s_{cr,\lim}$):

$L_b = s_{cr}$ (estimated crack distance)

- for long crack distances ($s_{cr} \geq s_{cr,\lim}$):

$L_b = s_{cr,\lim}$ (limit between a short and long crack distance)

$P_{\max,L=Lb}$: theoretical maximum transferred force of a pure shear specimen (equation (3.76)) whose length is equal to L_b

When the concrete's contribution in tension is not considered, the limit between a short and long crack distance can be explicitly expressed as equation (5.12). This expression is equivalent to equation (4.51) as specified for the maximum shear force. In other words, the maximum shear force has been incorporated into equation (4.51) through the υ function, resulting in equation (5.12).

$$s_{cr,\lim} = \frac{1}{\Omega_2} \arcsin\left(\frac{\tau_{LM} b_L}{\Omega_2 M\left(x = x_J\right)\left(1 - \frac{f_y A_s z_s}{M_y}\right)} z_L \right) \tag{5.12}$$

In addition, for $\kappa = 0$, the maximum shear force is simplified as follows:

$$V_{J,\max} = \frac{1}{s_{cr}\cos\left(\Omega_2 L_b\right)\left(1 - \frac{f_y A_s z_s}{M_y}\right)} \left\{ P_{\max,L=Lb} z_L - M\left(x = x_J\right)\left(1 - \frac{f_y A_s z_s}{M_y}\right) \right. \tag{5.13}$$
$$\left. \left(1 - \cos\left(\Omega_2 L_b\right)\right) \right\} - q\frac{s_{cr}}{2}$$

Case 2: $M(x = x_J) \geq M_y$ and $M(x = x_I) < M_y$ (Internal steel reinforcement yielded in crack J but not in crack I)

Once the internal steel yields in crack J, the limit between a short and long crack distance, $s_{cr,\lim}$, can be obtained for the maximum shear force by solving equation (5.14). This equation is similar to equation (5.9) except for the term that depends on the bending moment.

$$\frac{\tau_{LM} b_L}{\Omega_2} z_L + \frac{2\kappa A_L z_L}{\Omega_2^2 s_{cr,\lim}^2} \sin\left(\Omega_2 s_{cr,\lim}\right) - \frac{\kappa A_L z_L}{\Omega_2 s_{cr,\lim}} \left(1 + \cos\left(\Omega_2 s_{cr,\lim}\right)\right) - \tag{5.14}$$
$$- \left(M\left(x = x_J\right) - f_y A_s z_s\right) \sin\left(\Omega_2 s_{cr,\lim}\right) = 0$$

where:

κ: constant given by equation (5.10)

The maximum shear force that can be reached before a premature debonding of the laminate can be calculated as shown by equation (5.15) for each bending moment on

crack J higher than the yielding bending moment and lower than the bending moment that causes steel yielding in crack I.

$$V_{J,\max} = \frac{1}{s_{cr}\cos(\Omega_2 L_b)\left(1-\frac{f_y A_s z_s}{M_y}\right)}\left\{P_{\max,L=Lb} z_L + \frac{2\kappa A_L z_L}{\Omega_2^2 s_{cr}^2}(1-\cos(\Omega_2 L_b))\right.$$
$$\left. - \frac{\kappa A_L z_L}{\Omega_2 s_{cr}}\sin(\Omega_2 L_b) + f_y A_s z_s - M(x=x_J)\left(1-\cos(\Omega_2 L_b)\left(1-\frac{f_y A_s z_s}{M_y}\right)\right)\right\} - q\frac{s_{cr}}{2} \quad (5.15)$$

where:

L_b and $P_{\max,L=Lb}$ were defined in Case 1

The same comments of the previous case in relation to the crack distances are valid herein. When the concrete's contribution is not considered (κ = 0), both equations (5.14) and (5.15) can be simplified as follows.

$$s_{cr,\lim} = \frac{1}{\Omega_2}\arcsin\left(\frac{\tau_{LM} b_L}{\Omega_2\left(M(x=x_J) - f_y A_s z_s\right)} z_L\right) \quad (5.16)$$

$$V_{J,\max} = \frac{1}{s_{cr}\cos(\Omega_2 L_b)\left(1-\frac{f_y A_s z_s}{M_y}\right)}\left\{P_{\max,L=Lb} z_L + f_y A_s z_s - M(x=x_J)\right.$$
$$\left.\left(1-\cos(\Omega_2 L_b)\left(1-\frac{f_y A_s z_s}{M_y}\right)\right)\right\} - q\frac{s_{cr}}{2} \quad (5.17)$$

Case 3: $M(x = x_J) \geq M_y$ and $M(x = x_I) \geq M_y$ (Internal steel reinforcement yielded in both cracks I and J)

In this case, the limit between a short and long crack distance, $s_{cr,\lim}$, is calculated by solving equation (5.18), which coincides with equation (5.14).

$$\frac{\tau_{LM} b_L}{\Omega_2} z_L + \frac{2\kappa A_L z_L}{\Omega_2^2 s_{cr,\lim}^2}\sin(\Omega_2 s_{cr,\lim}) - \frac{\kappa A_L z_L}{\Omega_2 s_{cr,\lim}}(1+\cos(\Omega_2 s_{cr,\lim})) -$$
$$-\left(M(x=x_J) - f_y A_s z_s\right)\sin(\Omega_2 s_{cr,\lim}) = 0 \quad (5.18)$$

where:

κ: constant given by equation (5.10)

In addition, the maximum shear force prior to laminate peeling failure is obtained as shown by equation (5.19) for all bending moments on crack J higher than the value that causes steel yielding in crack I.

$$V_{J,\max} = \frac{1}{s_{cr}\cos(\Omega_2 L_b)}\left\{ P_{\max,L=Lb} z_L + \frac{2\kappa A_L z_L}{\Omega_2^2 s_{cr}^2}(1-\cos(\Omega_2 L_b)) - \right.$$
$$\left. - \frac{\kappa A_L z_L}{\Omega_2 s_{cr}}\sin(\Omega_2 L_b) - (M(x=x_J) - f_y A_s z_s)(1-\cos(\Omega_2 L_b)) \right\} - q\frac{s_{cr}}{2} \qquad (5.19)$$

where:

L_b and $P_{\max,L=Lb}$ were defined in Case 1

When neglecting the concrete's contribution in tension, $s_{cr,\lim}$ can be calculated from the more simplified equation (5.16), because equation (5.18) is equal to (5.14). In addition, equation (5.19) can be simplified to (5.20).

$$V_{J,\max} = \frac{1}{s_{cr}\cos(\Omega_2 L_b)}\left\{P_{\max,L=Lb} z_L - (M(x=x_J) - f_y A_s z_s)(1-\cos(\Omega_2 L_b))\right\}$$
$$- q\frac{s_{cr}}{2} \qquad (5.20)$$

Some general comments to the three cases described above are listed below:

1) Equations (5.11), (5.15) and (5.19) for the maximum shear force have been derived from the limit condition for the tensile stress in crack J given by equations (4.46) (short crack distances) and (4.65) (long crack distances), assuming that the tensile stress in crack I and in crack J are related through equation (4.42).
2) Since the governing equations for the laminate tensile stresses are very similar for both Stages 2b and 3b (see Chapter 4), the maximum shear force expression (given by equations (5.11), (5.15) or (5.19)) is the same for both stages. The only difference between them is the considered bonded length.
3) In a short crack distance, the estimated value for s_{cr} is lower than the limit $s_{cr,\lim}$ given by equations (5.9), (5.14), or (5.18). Thus, the maximum shear force $V_{J,\max}$ is calculated assuming the bonded length, L_b, equal to the estimated crack distance, s_{cr}.
4) For short crack distances ($s_{cr} < s_{cr,\lim}$), since s_{cr} is a constant value, equations (5.11), (5.15) and (5.19) linearly depend on the bending moment acting on crack J. The maximum shear force before peeling occurs is a decreasing function of crack J's bending moment. The slope of the straight lines given by (5.11) (Case 1) and (5.19) (Case 3) is in both cases equal to (1 - $\cos(\Omega_2 L_b)$). However, the slope of equation (5.15) (Case 2) is smoother than in the previous cases, since $\cos(\Omega_2 L_b)$ is multiplied by a factor lower than 1.0.
5) In a long crack distance, since the estimated crack distance, s_{cr}, is higher than the limit between a short and long crack distance, the maximum shear force $V_{J,\max}$ is calculated assuming L_b equal to the limit $s_{cr,\lim}$.

6) For long crack distances ($s_{cr} \geq s_{cr,\lim}$), the remaining bonded length, $s_{cr,\lim}$, depends on the bending moment acting on crack J (Figure 5.3). As long as the bending moment increases, the remaining bonded length associated to the maximum shear force will decrease.
7) The crack distance limit, $s_{cr,\lim}$, should always be lower than or equal to the limit length for a pure shear specimen as given by equation (3.34) of Chapter 3. This value is associated to a zero value in tensile force in crack I. Higher values of the crack distance limit imply a compressive laminate force acting on crack I, which has no meaning. Therefore, from equations (5.12) and (5.16), the crack distance limit should be limited by the following values:

$$0 \leq s_{cr,\lim} \leq \frac{\pi}{2\Omega_2} \tag{5.21}$$

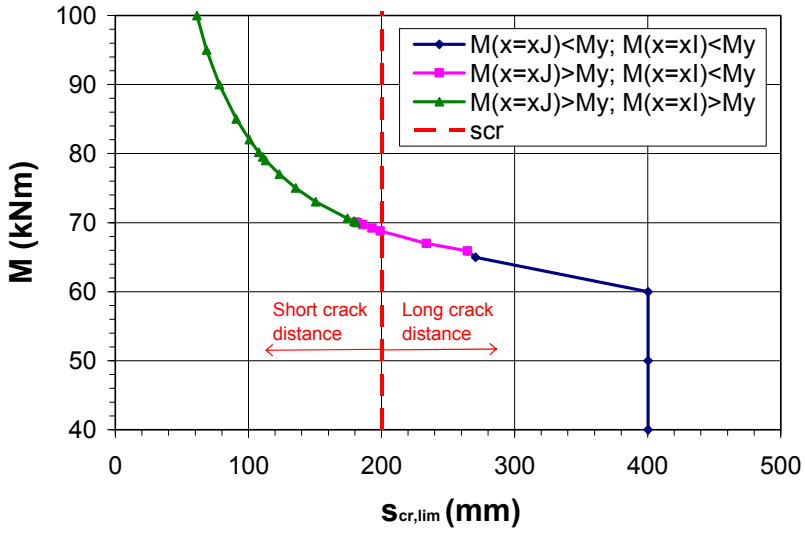

Figure 5.3. Crack distance limit.

8) For long crack distances, the maximum shear force depends on the remaining bonded length, which is variable. This is the main difference with short crack distances where the bonded length along the crack distance is a constant value. The maximum shear force in a long crack distance follows the same decreasing tendency as for short distances but in a non-linear manner.
9) Since the shear force decreases with increasing values of the bending moment, the maximum possible shear force can be obtained from Case 1, when the steel remains unyielded either in crack I or J.
10) Case 3 starts when the steel has yielded in both cracks I and J, that is when:

$$M(x = x_I) = M(x = x_J) - V_{J,\max} s_{cr} - q\frac{s_{cr}^2}{2} = M_y \tag{5.22}$$

By incorporating equation (5.22) into equation (5.19), the bending moment acting on crack J at this point can be stated as (5.23).

$$M\left(x=x_J\right)=M_y+\frac{1}{\cos\left(\Omega_2 L_b\right)}\left[P_{\max,L=Lb}\,z_L+\frac{2\kappa A_L z_L}{\Omega_2^2 s_{cr}^2}\left(1-\cos\left(\Omega_2 L_b\right)\right)-\right.$$
$$\left.-\frac{\kappa A_L z_L}{\Omega_2 s_{cr}}\sin\left(\Omega_2 L_b\right)+f_y A_s z_s\left(1-\cos\left(\Omega_2 L_b\right)\right)+q\frac{s_{cr}^2}{2}\cos\left(\Omega_2 L_b\right)\right] \tag{5.23}$$

11) In case the shear force is very large, the bending moment on crack I, which is calculated from the bending moment on crack J, as shown by equation (5.2), can be a negative number. Since the bending moment on crack I should always be higher than or equal to zero, the maximum shear force on crack J will have an upper limit given by equation (5.24).

$$V_{J,\max}\le\frac{M\left(x=x_J\right)}{s_{cr}}-q\frac{s_{cr}}{2} \tag{5.24}$$

12) This upper limit is a straight line which depends on the estimated crack distance. The slope of this line increases with increasing values of the crack distance. Usually, this upper limit intersects with the maximum shear force-bending moment relationship before steel yields in both cracks.
13) The bending moment on crack J should always be lower than the ultimate bending moment associated to concrete crushing or FRP rupture. If the bending moment related to Case 3 is higher than the value that causes a classic failure mode, no premature laminate debonding will be observed.
14) In a pure flexure case ($V = 0$), the bending moment that causes peeling failure is obtained when the sliding is at maximum (s_{L0}) along the whole crack distance. At this point, the bending moment acting on crack J is given by equation (5.25).

$$M_{peel,pureflexure}=\frac{2s_{L0}}{s_{cr}}E_L A_L z_L+f_y A_s z_s \tag{5.25}$$

15) Those cases with low values of shear force can almost be assumed as a pure flexural case. Thus, their maximum bending moment will be limited by the peeling moment given by equation (5.25).
16) Finally, the bending moment on crack J has an upper limit which consists of the lowest value of either the ultimate bending moment that causes concrete crushing or FRP rupture, or the bending moment associated to peeling failure in a pure flexure case. This upper limit is represented by a horizontal line that usually intersects the maximum shear force-bending moment curve once the internal steel has yielded in both cracks I and J.

$$M\left(x=x_J\right)_{\max}=\min\left\{M_u\left(\varepsilon_{cu}=3.5‰;\varepsilon_{Lu}\right);M_{peel,pureflexure}\right\}=$$
$$=M_u\left(\varepsilon_{cu}=3.5‰;\varepsilon_{Lu};\varepsilon_{L,pureflexure}=2s_{L0}/s_{cr}\right) \tag{5.26}$$

5.2.3. Examples to obtain the limit for the maximum shear force before peeling occurs

This section deals with some application examples of the previous formulae to obtain the limit relationship between the bending moment acting on crack J and the maximum shear force that can be reached assuming a maximum transmission of shear stresses along the interface between two cracks.

A beam loaded in a three-point bending configuration is studied. The geometry dimensions of the section and material properties are assumed to be equal to Beam 2 of the Experimental program described in Chapter 2. Therefore, the model parameters in this example are: τ_{LM} = 2.46 *MPa*, s_{LM} = 0.008 *mm*, and s_{L0} = 0.764 *mm*. After performing a moment-curvature analysis, the steel yield bending moment is found to be 65.9 *kNm*.

Example 1. Crack distance of 100 mm

A crack distance of 100 *mm* is first studied. The maximum shear force before peeling occurs is obtained by applying the procedure described in the following lines, for the three cases mentioned in §5.2.2. To clarify the following description, Figure 5.4 shows the relationship between the bending moment acting on crack J and the maximum shear force that can be reached assuming a maximum transmission of shear stresses along the interface.

Case 1: Steel is unyielded in both cracks I and J, $M(x = x_J) \leq 65.9$ *kNm*

1) The crack distance limit $s_{cr,\lim}$ for the maximum shear force is obtained by using equation (5.9). For a bending moment on crack J equal to M_y, the crack distance limit is 264 *mm*. Since the crack distance limit decreases with increases in applied bending moments (see Figure 5.3), the crack distance limit during Case 1 will always be higher than 264 *mm*. Therefore, the crack distance of 100 mm will be a short crack distance before steel yields at any location.
2) Since it is a short crack distance, the maximum transferred force is attained at the beginning of Stage 2b, and the maximum shear force varies in a linear manner with the bending moment.
3) The maximum shear force decreases from 237.6 *kN* (for $M(x = x_J) = 0$) to 182.9 *kN* (for $M(x = x_J) = M_y$).
4) The upper limit given by equation (5.22) crosses the limit line given above at 219.3 *kN*. At this point, the applied moment on crack J is 22.0 *kNm*.
5) Therefore, in this example, the Case 1's maximum shear force-bending moment relationship consists of two straight lines with different slopes. The maximum shear force increases linearly from a zero value to 219.3 *kN*, while the bending moment increases up to 22.0 *kNm*. Later on, for bending moments in crack J higher than 22.0 *kNm* and lower than M_y, the shear force limit decreases in a linear manner from 219.3 *kN* to 182.9 *kN*.

Case 2: Steel has yielded only in crack J, 65.9 $kNm \leq M(x = x_J) \leq 69.2$ kNm and $M(x = x_I) \leq 65.9$ kNm

1) The crack distance limit $s_{cr,\lim}$ decreases from 264 *mm* to 193 *mm* (equation (5.14)). Since the crack distance of 100 mm is lower than the minimum value, Case 2 is also a short crack distance.
2) The maximum shear force linearly decreases as the applied moment on crack J increases from the yield bending moment, 65.9 *kNm,* to a value that also yields the steel in crack I, 69.2 *kNm*.

Case 3: Steel has yielded in both cracks I and J, $M(x = x_J) \geq 69.2$ kNm and $M(x = x_I) \geq 65.9$ kNm

1) In this case, the crack distance limit $s_{cr,\lim}$ starts to decrease from the initial value of 193 *mm* (equation (5.18)). If the crack distance of 100 *mm* was always short during Case 3, the shear force would decrease from the value associated to a 69.2 *kNm* to a zero value. The zero shear force would correspond to an applied bending moment on crack J of 109.5 *kNm*. However, the crack distance limit associated to a zero shear force, $s_{cr,\lim}$ is 50.7 mm. This value indicates that the laminate, which has been considered short during Case 1 and 2, is no longer short. The bending moment above which the crack distance is considered long is equal to 82.0 *kNm*.
2) As a consequence, the maximum shear force will decrease in a linear manner while the distance is short, in other words, while the bending moment on crack J increases from 69.2 *kNm* to 82.0 *kNm.*
3) Once the bending moment on crack J reaches 82.0 *kNm*, the crack distance is considered long and the slope of the maximum shear force line increases significantly.
4) It should be mentioned that the bending moment in Case 3 has an upper limit which is the lowest value of either the ultimate bending moment due to concrete crushing or to laminate rupture, or to peeling failure in a pure flexure case. In this case, the bending moment that causes concrete to crush is equal to 79.5 *kNm.* In addition, the bending moment associated to peeling failure in a pure flexure case is equal to 110.6 *kNm*, which is lower than the bending moment that causes FRP rupture. The upper limit value is equal to 79.5 *kNm* and is represented by a horizontal line that intersects the maximum shear force of Case 3.
5) Since this upper limit is lower than the bending moment associated to the limit between short and long crack distances (see Figure 5.4), the crack distance is considered short for the whole maximum shear force-bending moment relationship given in this example.

Once the maximum shear force is obtained for any bending moment, it can be observed from Figure 5.4, that the plotted line divides the graph into two regions. If the binomial $(V, M)_{x=xJ}$ acting on crack J is below the plotted line, the laminate will still be attached and the peel-off phenomena will not have started. If this point is in the plotted line, the beam element between those two cracks, I and J, will have reached the maximum transferable force between laminate and support, so the external reinforcement will peel-off if the bending moment on crack J is increased. Finally, if this point is above the limit line, the laminate debonding process will have been previously initiated. The

different branches of the plotted line observed in Figure 5.4 correspond to the different cases discussed above.

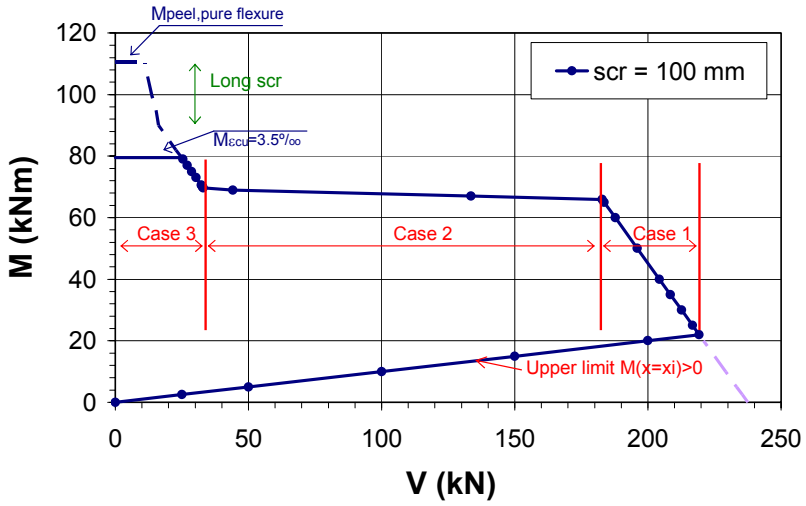

Figure 5.4. Shear force vs. bending moment for a 100 mm crack distance.

Example 2. Crack distance of 200 mm.

For a 200 *mm* crack distance, the relationship between the bending moment on crack J and the maximum shear force before a premature laminate debonding occurs is obtained in this example according to §5.2.2. Figure 5.5 plots this relationship and helps to understand the procedure description given below.

Case 1: Steel is unyielded in both cracks I and J, $M(x = x_J) \leq 65.9$ *kNm*

1) First, the crack distance limit $s_{cr,\lim}$ associated to the maximum shear force is calculated according to equation (5.9). As mentioned in the previous example, the crack distance limit during Case 1 is always higher than the value associated to the steel yield bending moment on crack J, which is 264 *mm*. Hence, the crack distance of 200 mm will be a short crack distance before steel yields at any location.
2) The maximum shear force during Case 1 decreases in a linear way with increasing values of the bending moment. The lower value of the maximum shear force, 150.9 *kN,* is associated to a bending moment that causes internal steel yielding in crack J ($M(x = x_J) = M_y$). As observed, in the previous example of a 100 *mm* crack distance, the maximum shear force associated to steel yielding in crack J (182.9 *kN*) was higher than the current value of 150.9 *kN*.
3) In a similar manner as in the previous example, the upper limit given by equation (5.21) crosses the limit line given above at 200.0 *kN*, when the applied moment on crack J is 40.0 *kNm*. Therefore, the maximum shear force increases linearly from a zero value to 200.0 *kN*, with increasing values of the bending moment up to 40.0 *kNm*. Later on, for bending moments in crack J higher than 40.0 *kNm* but lower than M_y, the shear force limit will decrease in a linear manner from 200.0 *kN* to 150.9 *kN*.

4) Note that the slope of this upper limit line is higher for a 200 *mm* crack distance than for a 100 *mm* crack distance (see the previous example). Hence, the higher the estimated crack distance, the higher the slope of the upper limit line.

Case 2: Steel has yielded only in crack J, 65.9 $kNm \leq M(x = x_J) \leq 70.1$ *kNm* and $M(x = x_I) \leq 65.9 kNm$

1) During Case 2, the crack distance limit $s_{cr,\lim}$ decreases from 264 *mm* to 174 *mm* (equation (5.13)). Since 200 *mm* is in between both values, the crack distance is considered short up to the point where the crack distance limit equals the estimated value (200 *mm*). In other words, the crack distance is considered short for bending moments acting on crack J lower than 68.8 *kNm*, (associated to $s_{cr,\lim} = 200$ *mm*). Beyond this bending moment value, the crack distance is considered long.
2) For both short and long crack distances, the maximum shear force will decrease as long as the applied moment on crack J increases from 65.9 *kNm,* to the value that yields the steel in crack I, which is 70.1 *kNm*.
3) While difficult to appreciate, in Figure 5.5, the slope of the maximum shear force line slightly increases once the crack distance is considered long.

Case 3: Steel has yielded in both cracks I and J, $M(x = x_J) \geq 70.1$ *kNm* and $M(x = x_I) \geq 65.9$ *kNm*

1) Since the crack distance limit $s_{cr,\lim}$ starts to decrease from 181 *mm* as the moment on crack J increases (equation (5.17)), the 200 *mm* crack distance is considered long during Case 3.
2) The maximum shear force decreases in a non-linear way as the applied moment on crack J increases above 70.1 *kNm*.
3) As in the previous example, Case 3 has an upper limit which is the minimum value of either the ultimate bending moment due to concrete crushing (79.5 *kNm*) or the peeling bending moment of a pure flexure case (81.1 *kNm*). This upper limit is represented by a horizontal line that intersects Case 3.
4) In this case, note that the peeling bending moment of a pure flexure case is lower than the value obtained for a 100 *mm* crack distance.

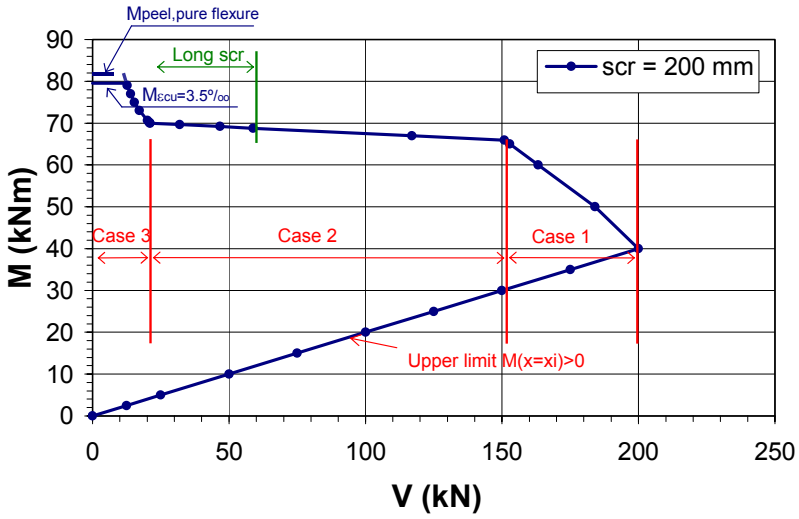

Figure 5.5. Shear vs. bending moment for a 200 mm crack distance.

5.2.4. Simplified maximum shear force vs. bending moment relationship to prevent peeling failure

The procedure, described in §5.2.2, to obtain the shear force limit that prevents peeling failure may be complicate during the design of an external reinforcement. This section presents some simplifications derived from the analysis of some cases including the previous examples.

For short and long crack distances, the influence of the concrete's contribution in tension in the maximum shear force-bending moment relationship has been analyzed. Although results are not presented here, the main conclusion is that the influence of concrete in tension is not significant. Therefore, from now on, the concrete's contribution in tension will be neglected to simplify the design procedure.

As shown in §5.2.2, when the estimated crack distance s_{cr} is considered short ($s_{cr} < s_{cr,\lim}$), the maximum shear force is related to the bending moment on crack J linearly. The slope of this linear relationship varies depending on the steel state. For a long crack distance, ($s_{cr} \geq s_{cr,\lim}$), the maximum shear force-bending moment relationship becomes non-linear since it depends on a variable crack distance limit $s_{cr,\lim}$. In case the relationship is approached using linear functions for each different case, the committed error is very low. In addition, the upper limit, which prevents having a negative moment value on crack I, is linear as well for any crack distance. Furthermore, the other upper limit associated to a classic failure or to a pure flexure case is a horizontal line. As a consequence, the simplified maximum shear force-bending moment relationship can be approached by a multi-linear function.

The procedure to obtain a simplified shear force limit is described as follows:

1) First, the average crack distance is determined as mentioned in §5.2.2.

2) Then, the simplified maximum shear force-bending moment relationship is defined by some key points (shown in Figure 5.6) given by the multi-linear function branch ends.

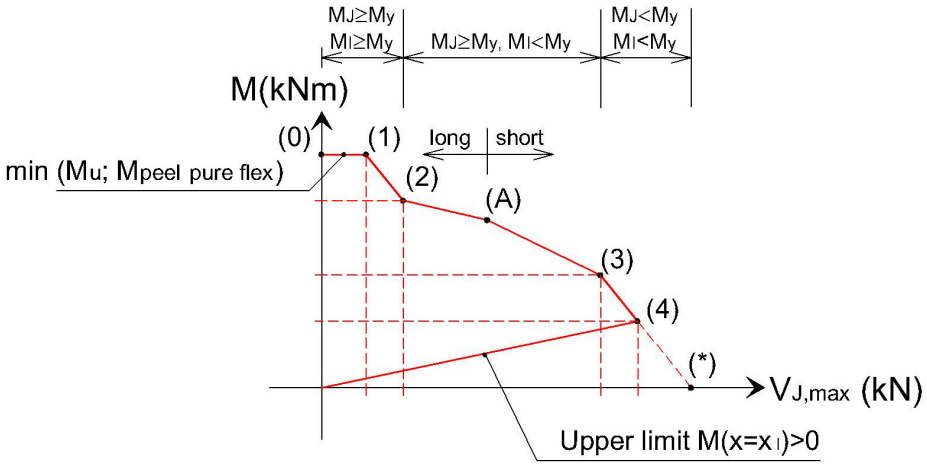

Figure 5.6. Simplified maximum shear force vs. bending moment relationship.

3) The formulae to obtain these significant points, together with a description of their importance, are given below. The crack distance limit $s_{cr,\lim}$ should be obtained at point (1), by using equation (5.16), and at both points (2) and (3) by applying equation (5.12). By comparing the estimated crack distance to this limit value, the crack distance is identified as short ($s_{cr} < s_{cr,\lim}$) or long ($s_{cr} \geq s_{cr,\lim}$). In case the crack distance is short, the bonded length L_b will be equal to the estimated crack distance, s_{cr}. On the contrary, if the crack distance is long, L_b will be equal to the limit between a short and long crack distance $s_{cr,\lim}$.

Point (0): The bending moment on crack J should be lower than the lowest value of either the ultimate bending moment that causes concrete to crush or laminate to rupture, or peeling failure in a pure flexure case.

$$V_{J,\max}^{(0)} = 0 \tag{5.27}$$

$$M_{J,\max}^{(0)} = M_u\left(\varepsilon_{cu} = 3.5‰; \varepsilon_{Lu}; \varepsilon_{L,pureflexure} = 2\,s_{L0}/s_{cr}\right) \tag{5.28}$$

Point (1): The intersection of the bending moment given by (5.28) with the branch where the internal steel is yielded in both cracks I and J gives the maximum shear force that can be reached during Case 3 (see equation (5.30)). The crack distance limit for point (1) (equation (5.29)) can be obtained after incorporating equation (5.28) into equation (5.16).

$$s_{cr,\lim}^{(1)} = \frac{1}{\Omega_2}\arcsin\left(\frac{\tau_{LM} b_L}{\Omega_2\left(M_{J,\max}^{(1)} - f_y A_s z_s\right)} z_L\right) \tag{5.29}$$

$$V_{J,\max}^{(1)} = \frac{1}{s_{cr}\cos(\Omega_2 L_b)}\left\{P_{\max,L=Lb} z_L - \left(M_{J,\max}^{(1)} - f_y A_s z_s\right)\left(1-\cos(\Omega_2 L_b)\right)\right\} - q\frac{s_{cr}}{2} \quad (5.30)$$

$$M_{J,\max}^{(0)} = M_u\left(\varepsilon_{cu} = 3.5‰; \varepsilon_{Lu}; \varepsilon_{L,pureflexure} = 2\,s_{L0}/s_{cr}\right) \quad (5.31)$$

Point (2): The shear force given by Point (2) is the maximum value that can be reached when the applied moment on crack J yields the internal steel in crack I. Similar to point (1), the crack distance limit should be obtained (equation (5.32)) in order to classify the estimated crack distance into short or long.

$$s_{cr,\lim}^{(2)} = \frac{1}{\Omega_2}\arctan\left(\frac{\tau_{LM} b_L}{\Omega_2\left(M_y - f_y A_s z_s\right)} z_L\right) \quad (5.32)$$

$$V_{J,\max}^{(2)} = \frac{1}{s_{cr}}\left\{P_{\max,L=Lb} z_L - \left(M_y - f_y A_s z_s\right)\left(1-\cos(\Omega_2 L_b)\right)\right\} - q\frac{s_{cr}}{2} \quad (5.33)$$

$$M_{J,\max}^{(2)} = M_y + V_{J,\max}^{(2)} s_{cr} = P_{\max,L=Lb} z_L + M_y\cos(\Omega_2 L_b) + f_y A_s z_s\left(1-\cos(\Omega_2 L_b)\right) \quad (5.34)$$

Point (3): Point (3) gives the maximum shear force associated to an applied bending moment on crack J equal to M_y. For this point, the crack distance limit is obtained as shown by equation (5.35).

$$s_{cr,\lim}^{(3)} = \frac{1}{\Omega_2}\arcsin\left(\frac{\tau_{LM} b_L}{\Omega_2\left(M_y - f_y A_s z_s\right)} z_L\right) \quad (5.35)$$

$$V_{J,\max}^{(3)} = \frac{P_{\max,L=Lb} z_L - \left(M_y - f_y A_s z_s\right)\left(1-\cos(\Omega_2 L_b)\right)}{s_{cr}\cos(\Omega_2 L_b)\left(1 - \frac{f_y A_s z_s}{M_y}\right)} - q\frac{s_{cr}}{2} \quad (5.36)$$

$$M_{J,\max}^{(3)} = M_y \quad (5.37)$$

Point (*): Auxiliary point associated to a zero bending moment value on crack J. It is obtained in order to find the intersection of the upper limit, given by equation (5.24), with the maximum shear force.

$$V_{J,\max}^{(*)} = \frac{P_{\max,L=scr} z_L}{s_{cr}\cos(\Omega_2 s_{cr})\left(1 - \frac{f_y A_s z_s}{M_y}\right)} - q\frac{s_{cr}}{2} \quad (5.38)$$

$$M_{J,\max}^{(*)} = 0 \quad (5.39)$$

4) Note that, usually, $M_{J,\max}^{(1)}$ is higher than $M_{J,\max}^{(2)}$. Therefore, the horizontal branch defined by points (1) and (2) almost always intersects the line of Case 3. Exceptionally, it intersects the line of Case 2. This fact has been observed when analyzing the bending test database given in Chapter 2.
5) The crack distance limit should be determined for points (1) to (3) by using equations (5.29), (5.32) and (5.35). If the crack distance, s_{cr}, in point (i) is short and in point (i+1) is long, there will be an intermediate point, known as (A), which is placed between (i) and (i+1) and where the crack distance turns from short to long. At point (A), the estimated crack distance s_{cr} is equal to the limit $s_{cr,\lim}$. Depending on the location of point (A), the shear force and bending moment associated to this point can be defined as follows:

Point (A) is in Case 1 (between (3) and (*)):

$$V_{J,\max}^{(A.1)} = \frac{1-\cos(\Omega_2 s_{cr})}{s_{cr}\sin(\Omega_2 s_{cr})\left(1-\frac{f_y A_s z_s}{M_y}\right)}\frac{\tau_{LM} b_L}{\Omega_2} z_L - q\frac{s_{cr}}{2} \tag{5.40}$$

$$M_{J,\max}^{(A.1)} = \frac{\tau_{LM} b_L}{\Omega_2\left(1-\frac{f_y A_s z_s}{M_y}\right)\sin(\Omega_2 s_{cr})} z_L \tag{5.41}$$

Point (A) is in Case 2 (between (2) and (3)):

$$V_{J,\max}^{(A.2)} = \frac{f_y A_s z_s}{s_{cr}} + \frac{1}{s_{cr}\left(1-\frac{f_y A_s z_s}{M_y}\right)}\frac{\tau_{LM} b_L}{\Omega_2} z_L \frac{\left(1-\frac{f_y A_s z_s}{M_y}\right)-\cos(\Omega_2 s_{cr})}{\sin(\Omega_2 s_{cr})} - q\frac{s_{cr}}{2} \tag{5.42}$$

$$M_{J,\max}^{(A.2)} = \frac{\tau_{LM} b_L}{\Omega_2 \sin(\Omega_2 s_{cr})} z_L + f_y A_s z_s \tag{5.43}$$

Point (A) is in Case 3 (between (1) and (2)):

$$V_{J,\max}^{(A.3)} = \frac{1-\cos(\Omega_2 s_{cr})}{s_{cr}\sin(\Omega_2 s_{cr})}\frac{\tau_{LM} b_L}{\Omega_2} z_L - q\frac{s_{cr}}{2} \tag{5.44}$$

$$M_{J,\max}^{(A.3)} = \frac{\tau_{LM} b_L}{\Omega_2 \sin(\Omega_2 s_{cr})} z_L + f_y A_s z_s \tag{5.45}$$

Figure 5.7 shows the three possible situations of Point (A), that is, the transition point between a short and long crack distance. Note that if Point (A) does not exist in the peeling limit line, the crack distance will be short regardless of the bending moment or shear force on crack J.

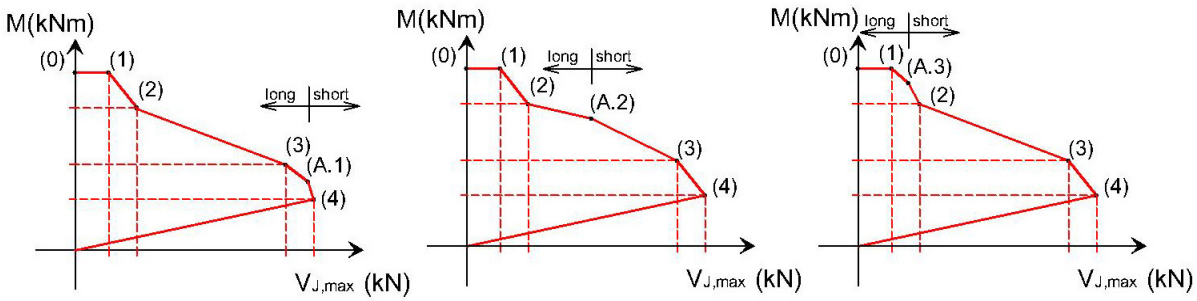

Figure 5.7. Shear force vs. bending moment relationship. Point (A) location.

6) As shown in the previous examples, the relationship between shear force and bending moment is bounded by an upper limit given by equation (5.24), to ensure that the bending moment on crack I is greater than or equal to zero. Point (4) is defined as the intersection of the line assigned to Case 1 or Case 2 with the upper limit line. It should be noted that there was not observed any test on the database where the upper limit line intersected the line of Case 3. The maximum shear force on point (4) in a three or four-point bending configuration can be written as a function of the shear force and bending moments of the neighboring points (i) and (i+1) (see equation (5.46)). The bending moment on point (4) is related to the maximum shear force by equation (5.47).

$$V_{J,\max}^{(4)} = \left(M_{J,\max}^{(i)} + \frac{M_{J,\max}^{(i)} - M_{J,\max}^{(i+1)}}{V_{J,\max}^{(i+1)} - V_{J,\max}^{(i)}} V_{J,\max}^{(i)} - q\frac{s_{cr}^2}{2} \right) \frac{1}{s_{cr} + \dfrac{M_{J,\max}^{(i)} - M_{J,\max}^{(i+1)}}{V_{J,\max}^{(i+1)} - V_{J,\max}^{(i)}}} \tag{5.46}$$

$$M_{J,\max}^{(4)} = V_{J,\max}^{(4)} s_{cr} + q\frac{s_{cr}}{2} \tag{5.47}$$

7) Depending on the location of point (A) and on the location of point (4), seven different simplified maximum shear force-bending moment relationships can be obtained. Schematic profiles of these relationships are given in Figure 5.8. Note that the possible situations of $M_{J,\max}^{(1)}$ being lower than $M_{J,\max}^{(2)}$ and of point (4) being in Case 3 are not considered, since both were not observed in the bending test database. As previously mentioned, the plotted line divides the graph into two regions. If the pair of shear force and bending moment on crack J $(V_d,\ M_d)_{x=xJ}$ is below the plotted line, the laminate will still be attached and peeling failure will not be observed. If this point is above the plotted line, the external reinforcement peels-off.

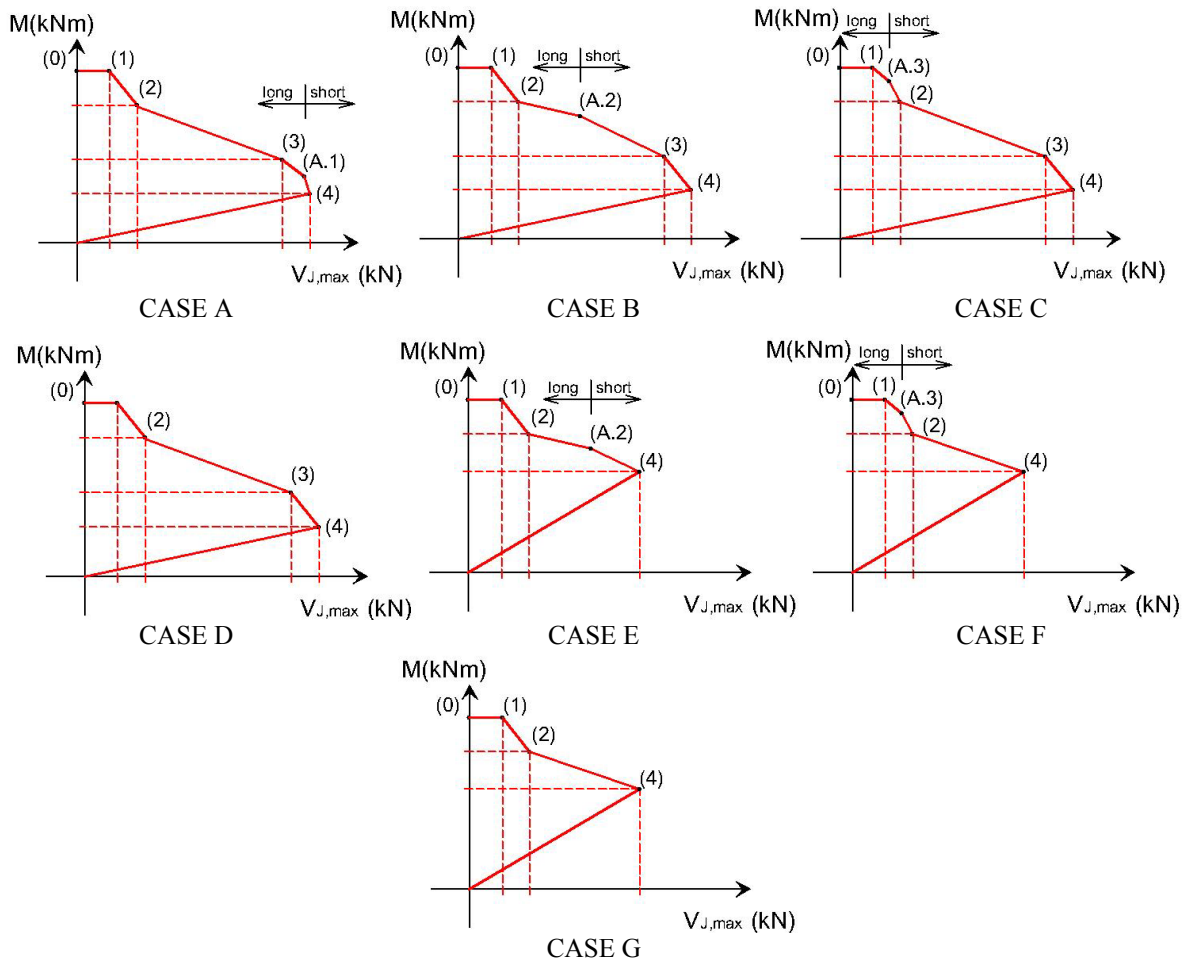

Figure 5.8. Possible cases for the shear force vs. bending moment relationship.

5.3. Verification procedure

Peeling may initiate at any location of the beam span due to the effect of flexural or shear cracks, or at the laminate end due to a high stress concentration. The verification procedure should check for peeling failure at every location. For this purpose, peeling failure initiated near cracks is checked at the most unfavorable section by comparing the experimental maximum shear force to the theoretical value that prevents the external reinforcement from debonding. Afterwards, peeling failure is checked at the laminate end. In some cases, this last checking step can lead into a readjustment of the maximum shear force predicted for peeling initiated near cracks. A detailed description of the verification procedure is given in the following paragraphs by distinguishing the initiation of the debonding process.

Peeling due to the effect of cracks

First, the most unfavorable section must be identified to check peeling failure near cracks. In a three-or-four-point bending situation the shear force is constant along the shear span, and the maximum bending moment is obtained under the load application

point. Therefore, the load application point results the most unfavorable section. After estimating the crack distance, s_{cr}, peeling failure is checked in an element between two cracks whose length is s_{cr}. In the studied element, the most loaded crack is under the load application point.

Then, the peeling shear force-bending moment relationship allows us to obtain the maximum shear force that can be attained before peeling occurs. Since the committed error is negligible, the simplified maximum shear force-bending moment relationship, defined in §5.2.4, is used in the verification procedure. For this purpose, four key points previously defined in addition to the transition between a short and long crack distance (point A) should be calculated. The theoretical maximum shear force vs. bending moment relationship corresponds to one of the possible cases given in Figure 5.8. The intersection of the experimental with the theoretical shear force-bending moment relationship gives the predicted maximum shear force that can be reached before peeling occurs due to cracks under the load application point, $V_{J,\max}$.

To find this intersection, the following procedure should be done. For each key point, the arc tangent of the quotient between the bending moment and the shear force is calculated.

$$\theta^{(i)} = \arctan\left(\frac{M_{J,\max}^{(i)}}{V_{J,\max}^{(i)}}\right) \tag{5.48}$$

By sorting out the angles associated with points (1) to (4) and with point (A), the studied limit relationship is identified as one of the seven possible cases described in §5.2.4. Then, the angle associated with the experimental failure load, $\theta_{\exp}$, is calculated as equation (5.49).

$$\theta_{\exp} = \arctan\left(\frac{M_{\exp}}{V_{\exp}}\right) \tag{5.49}$$

In a three or four-point bending configuration, the relationship between the experimental shear force and the maximum bending moment at the load application point is a straight line with a slope equal to the shear span, L_{shear}. Therefore, in this case, $\theta_{\exp}$ is equal to the arc tangent of the shear span.

$$\theta_{\exp} = \arctan\left(L_{shear}\right) \tag{5.50}$$

The angle associated with the experimental failure load, $\theta_{\exp}$, is compared to the angles obtained for the key points. Such a comparison gives an idea of the situation at failure, in other words, whether the internal steel has yielded or not in crack J or/and crack I. After identifying the location of $\theta_{\exp}$, the intersection point of the experimental line given by $\theta_{\exp}$ with the shear force limit line is then calculated using equation (5.51), where points (i) and (i+1) are the key points in between which is $\theta_{\exp}$.

$$V_{J,\max} = \left(M_{J,\max}^{(i)} + \frac{M_{J,\max}^{(i)} - M_{J,\max}^{(i+1)}}{V_{J,\max}^{(i+1)} - V_{J,\max}^{(i)}} V_{J,\max}^{(i)} \right) \frac{1}{L_{shear} + \frac{M_{J,\max}^{(i)} - M_{J,\max}^{(i+1)}}{V_{J,\max}^{(i+1)} - V_{J,\max}^{(i)}}} \tag{5.51}$$

In a four point-bending configuration, there is a region between the load application points where the shear force is zero and the bending moment is constant. This pure flexure zone behaves as shown in §4.3.7. Peeling failure will initiate between two flexural cracks in this area if the maximum sliding is reached along the whole crack distance. Peeling failure in a pure flexure zone is directly considered in the verification procedure because the bending moment that causes peeling failure in this zone constitutes an upper limit of the peeling shear force-bending moment relationship. Only for long shear spans (associated to high values of $\theta_{\exp}$), peeling failure in a pure flexure area can be critical.

As a conclusion of the previous discussion, the maximum shear force before peeling initiates near cracks is equal to the intersection between the experimental shear force vs. bending moment relationship and the peeling limit relationship described in §5.2.4.

$$V_{cracks} = V_{J,\max} \tag{5.52}$$

Peeling verification at the laminate end

During the verification procedure, it should not be forgotten that peeling may also initiate at the laminate end. For this reason, an additional check should be performed. First, with this in mind, the cracking bending moment is calculated according to the FIB Task Group 9.3 FRP (2001). Assuming that the predicted maximum shear force, V_{cracks}, is acting on the beam, the section where the bending moment is equal to the cracking moment M_{cr} can be identified. The distance between this section and the laminate end is calculated as $L_{b,end}$. If the calculated distance is negative, the first crack along the beam associated to the maximum shear force will appear along the unbonded length. In this case, the first crack in the bonded laminate length should be obtained. This is done by assuming the crack distance after the first crack in the unbonded length. If necessary the crack distance will be multiplied by a factor until one crack falls within the laminate. Then, the distance from the first crack in the bonded length to the laminate end is identified as $L_{b,end}$. The theoretical maximum transferred force along $L_{b,end}$ is calculated according to §4.4.6 of Chapter 4 as $P_{\max,L=Lb,end}$. The laminate tensile force under the first crack within the laminate length ($\sigma_{L,J\ end}\ A_L$) is obtained for the maximum shear force that prevents failure between cracks (V_{cracks}) through the use of a moment-curvature analysis.

If the laminate tensile force at the first crack in the bonded length is lower than the theoretical maximum transferred force, failure will initiate due to the effects of existing cracks and no failure at the laminate end will be observed. Therefore, the maximum shear force before peeling occurs will be equal to equation (5.53).

$$\sigma_{L,J\ end} A_L \le P_{\max,L=Lb,end} \quad \rightarrow ok \quad \rightarrow V_{pred} = V_{cracks} \tag{5.53}$$

If the laminate tensile force at the first crack in the bonded length is higher than the maximum transferred force, the external reinforcement will debond partially at the laminate end. This localized failure does not necessarily imply the complete laminate debonding, especially for those cases with short distances between the first crack and the laminate end, $L_{b,end}$ (see Figure 5.9).

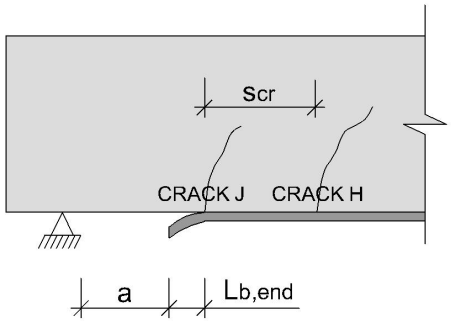

Figure 5.9. Local Failure at the laminate end.

An additional verification should be performed in case the laminate locally debonds at the end. Under these circumstances, the crack distance located from the first crack in the laminate (crack J) to the next crack towards midspan will be verified. The laminate tensile force in the second crack (crack H) is compared to the theoretical maximum transferred force along the crack distance, s_{cr}. The theoretical maximum transferred force is calculated according to §4.4.6 of Chapter 4, for an element at the laminate end whose length is the crack distance.

If the tensile force in crack H is lower than the theoretical maximum transferred force, the external reinforcement will peel-off due to the effect of cracks near midspan or near the load application point. In addition, a local debonding of the laminate end will be observed in this case.

$$\sigma_{L,H\,(H-J)} A_L \le P_{\max,L=scr} \quad \rightarrow ok \quad \rightarrow V_{pred} = V_{cracks} \tag{5.54}$$

In case the tensile force in crack H exceeds the maximum transferred force between cracks J and H, the laminate will completely debond from the laminate end towards midspan. Peeling failure will initiate for a shear force lower than V_{crack}. Thus, a more restrictive value of the predicted maximum shear force, V_{end}, should be obtained.

$$\sigma_{L,H\,(H-J)} A_L > P_{\max,L=sr} \quad \rightarrow V_{pred} = V_{end} \tag{5.55}$$

The theoretical maximum transferred force along the crack distance, $P_{\max,L=scr}$, gives the maximum laminate tensile force that can be attained in crack H. The bending moment associated to the tensile force in crack H can be obtained from the moment-curvature analysis. Since the location of crack H is known data, the shear force that causes peeling failure at the laminate end can be obtained as shown by equation (5.56).

$$\sigma_{L,H\,(H-J)} A_L = P_{\max,L=sr} \quad \rightarrow M_{crack\,H} \quad \rightarrow V_{pred} = V_{end} = \frac{M_{crack\,H}}{a + L_{b,end} + s_{cr}} \tag{5.56}$$

Once the predicted maximum shear force before peeling occurs is calculated, the final step of the verification procedure consists of comparing the experimental maximum shear force at the most unfavorable location to the theoretical prediction. If the experimental value is lower than the prediction, no peeling failure will be observed. On the contrary, the laminate will peel-off due to the effect of cracks or at the laminate end. Figure 5.10 summarizes the steps that should be followed during the verification procedure.

As an example, the verification procedure has been applied to Beams 1/A, 1/B, 1/C and 1/D of the experimental program described in Chapter 2, as shown in Figure 5.11. During the three-point bending test, an average crack spacing of 150 *mm* was observed. First, the experimental shear force at failure has been compared to the maximum shear force before peeling failure initiates near flexural or shear cracks, known as V_{cracks}. In order to do so, the relationship between the maximum shear force and the bending moment on crack J must be obtained by assuming that crack J is located at midspan and crack I is placed at a distance from crack J equal to the experimental average value for the crack spacing. The maximum shear force limit line of Beam group 1 corresponds to Case C of Figure 5.8. The transition between a short and long crack distance is associated to a bending moment of 55.5 *kNm*. As observed in Figure 5.11, point (A) is in the branch where the internal steel has yielded in both cracks. In addition, the upper limit line that restrains the bending moment on crack I to a positive value intersects the maximum shear force function in the branch where the internal steel remains elastic at every location. The intersection of the experimental shear force vs. bending moment relationship (plotted in Figure 5.11) with the theoretical limit line gives the maximum shear force that can be attained before peeling occurs near cracks, V_{cracks}. In this example, V_{cracks} is equal to 50.0 *kN*.

The experimental values of shear force and bending moment associated to the failure load at midspan $(V_{u,exp}, M_{u,exp})_{x=L/2}$ are also plotted in Figure 5.11 for Beams 1/A, 1/B, 1/C, and 1/D. It can be observed that Beam 1/D probably did not fail due to the peeling effect between two cracks, because the pair of shear force - bending moment is placed below the limit line. Since the pair $(V_{u,exp}, M_{u,exp})_{x=L/2}$ in Beams 1/A, 1/B and 1/C is over the limit line, it appears that the corresponding failure can be explained by the stress concentration around the cracks..

An additional verification has been performed at the laminate end. For the maximum theoretical shear force before peeling occurs (V_{cracks}), the distance from the laminate end to the cracking bending moment section, $L_{b,end}$, is calculated as 78 *mm* for Beams 1/A, 1/B and 1/C. The maximum transferred force along $L_{b,end}$ is 19.0 *kN*. Since the tensile force in the laminate at this location is 14.1 *kN*, a value lower than the maximum transferred force, peeling failure will first start near midspan.

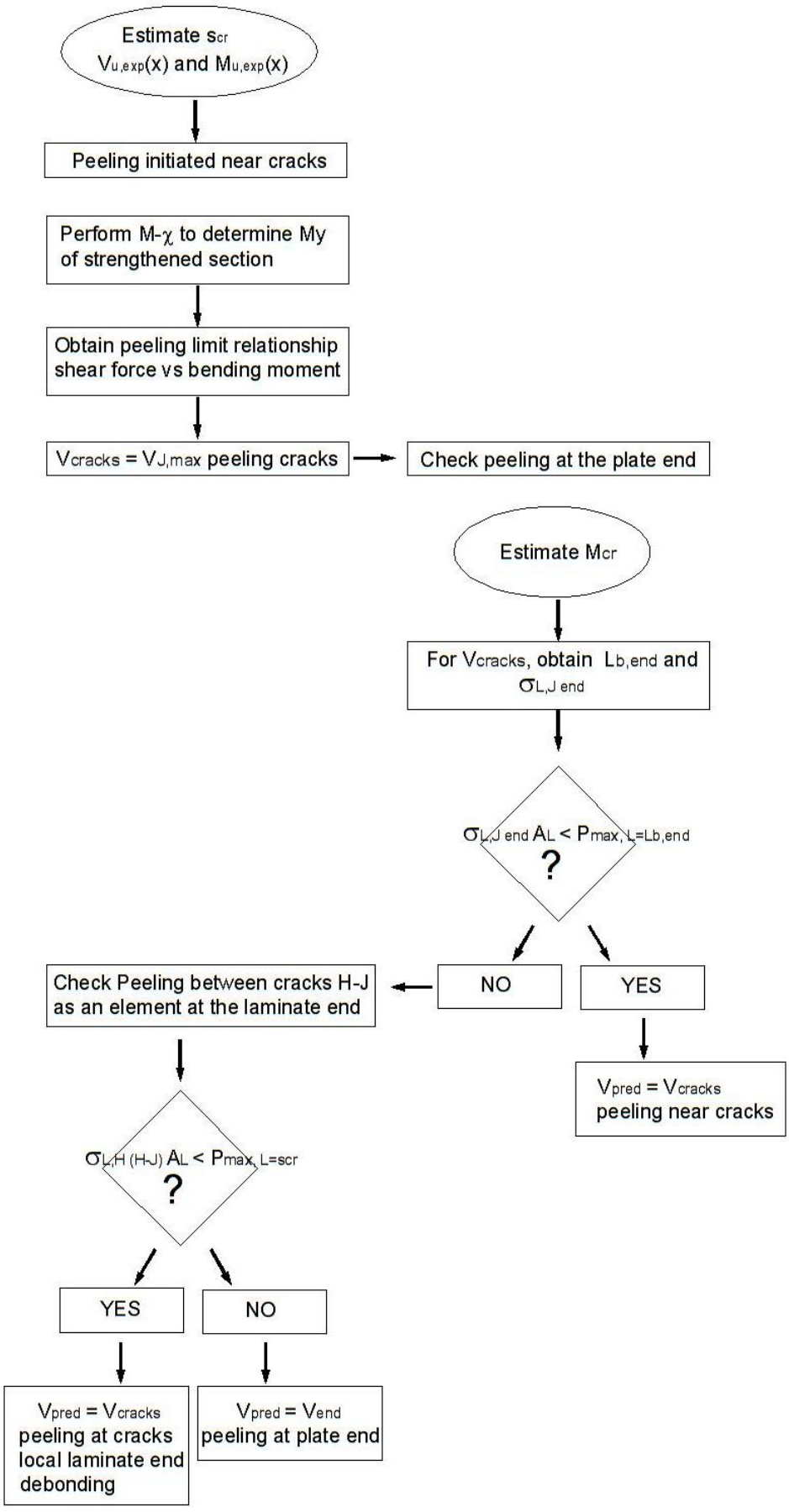

Figure 5.10. Verification procedure steps.

The unbonded length in Beam 1/D (250 *mm*) was longer than in the rest of Beams 1 (100 *mm*). The first crack associated to the maximum theoretical shear force in Beam 1/D appears along the unbonded length. The nearest crack (crack J) is already located in a bonded area. The distance between crack J and the laminate end is 122 *mm*. When the shear force that causes peeling near cracks is acting on the beam, the bending moment on crack J is 18.6 *kNm*. From the moment-curvature analysis the laminate tensile force associated to an 18.6 *kNm* bending moment is 29.5 *kN*, which is slightly lower than the theoretical maximum transferred force of 29.6 *kN*. Since both forces are very similar, the initiation of peeling failure cannot be stated for certain. Therefore, peeling may occur at the laminate end or near cracks.

If the tensile force in crack J was higher than the theoretical maximum transferred force, the verification procedure would have continued by checking the element between crack J and the nearest crack. If the tensile force in the most loaded crack was higher than the maximum transferred force along the crack distance, the predicted shear force would have been readjusted.

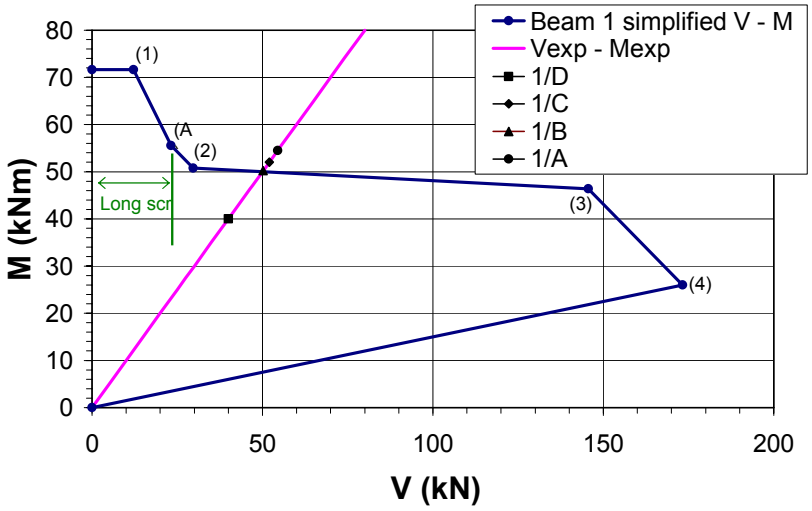

Figure 5.11. Shear vs. bending moment relationship for Beam group 1.

The verification procedure has also been applied to Beam group 2 of the experimental program performed by the author. The maximum shear force before peeling initiates near cracks is shown in Figure 5.12. This plot is associated to an observed average crack distance of 100 *mm*. The crack distance is identified as short for any bending moment on crack J (Case D). Since all beams in Beam group 2 were loaded in a three-point bending configuration, the critical section of study was midspan. The intersection of the experimental shear force-bending moment relationship at midspan with the peeling limit line of Figure 5.12 gives the theoretical maximum shear force before peeling occurs near midspan as 66.7 *kN*. The experimental values of shear force and bending moment under failure load at midspan $(V_{u,\exp}, M_{u,\exp})_{x=L/2}$ are plotted in Figure 5.12 for beams without external anchorage devices (2/C and 2/D). As observed, Beam 2/C probably failed due to the peeling effect. In addition, Beam 2/D is close to the limit line.

The laminate end has been verified while the maximum shear force of 66.7 *kN* was acting on the beam. The first crack is located at a distance of 34 *mm* from the laminate end. A moment-curvature analysis of Beam 2 gives a tensile force of 10.6 *kN* for the

cracking moment. This tensile force is higher than the maximum transferred force of 8.3 *kN* at the laminate end. Thus, the laminate will locally debond along 34 *mm*, and an additional verification should be performed to evaluate whether the laminate peeling-off is a localized phenomenon along $L_{b,end}$, or if it is a global phenomenon. The element between the first and the nearest crack at the laminate end is then checked. Since the laminate debonded along $L_{b,end}$, the laminate end is assumed to be located at the first crack. The tensile force in the second crack (crack H) is equal to 18.6 *kN* which is lower than the maximum transferred force of 24.0 *kN* at the laminate end for an element whose length is the average crack distance (100 *mm*). As a consequence, only a localized peeling failure at the laminate end is observed before the predicted shear force value for peeling near cracks is reached.

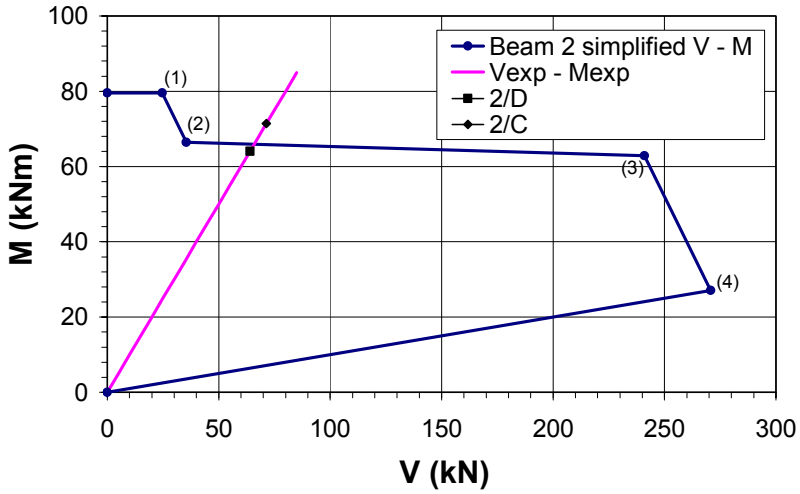

Figure 5.12. Shear vs. bending moment relationship for Beams 2.

The influence of crack distance in the maximum shear force vs. bending moment relationship is studied in Figure 5.13 for Beam group 1. The limit line for the observed 150 *mm* crack distance is compared to the limit lines associated to the values which were calculated according to the guidelines of FIB Task Group 9.3 FRP, 193 *mm*, and to the Spanish Structural Concrete Code, 125 *mm*. The main differences between the plotted lines are their slopes before steel yields and the slopes of the upper limit line. In addition, the maximum shear forces associated to the steel yield bending moment on both cracks I and J (points (2) and (3)) slightly increases with decreasing values of the crack distance. Therefore, the longer the crack distance, the more the conservative maximum shear force vs. bending moment relationship on crack J is.

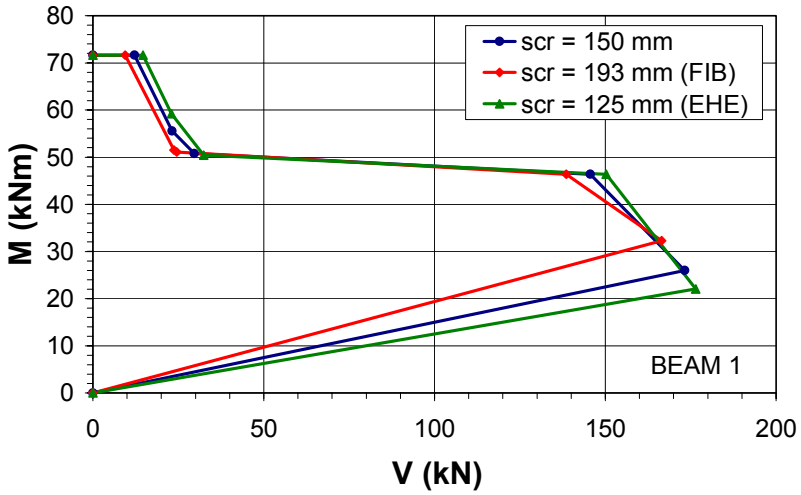

Figure 5.13. Shear force vs. bending moment for Beams 1 with different crack spacings.

Finally, Figure 5.14 shows that a 20% estimation error for the fracture energy does not have a significant influence on the relationship between shear force and bending moment. However, when the fluctuation represents 50% of the fracture energy, the difference is more noticeable, especially in the branch were the internal steel remains linear elastic. As observed, the experimental shear force vs. bending moment relationship intersects the limit line in the branch where the internal steel has yielded in crack J and remains linear elastic in crack I. Since the fracture energy fluctuation does not have a significant influence in this branch, the predicted value for the shear force is very similar regardless of the fracture energy value.

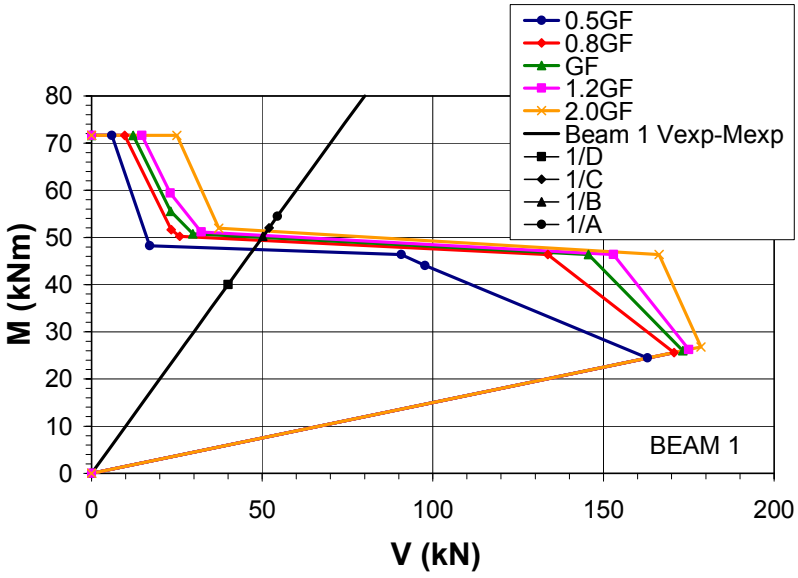

Figure 5.14. Influence of the fracture energy on the shear force vs. bending moment relationship.

5.4. Design procedure

In the following lines, the design procedure to estimate the necessary laminate area to strengthen an existing reinforced concrete section is explained. Firstly, an assumption of the existing loads acting on the unstrengthened structural element is made. The design moment of the unreinforced section, $M_{d,0}$, is calculated as a function of the existing loads. The ultimate bending moment of the unreinforced section, $M_{u,0}$, can be found by using equation (5.57).

$$M_{u,0} = T_s d\left(1 - \frac{T_s}{2C_c}\right) \tag{5.57}$$

where:

$$T_s = A_s f_{yd} \tag{5.58}$$

$$C_c = 0.85 f_{cd} bd \tag{5.59}$$

Equation (5.60) gives the height of the compression block, y_0, which the neutral axis depth is derived from (x_0).

$$y_0 = \frac{T_s}{C_c} d \tag{5.60}$$

Secondly, the design situations and load combinations after strengthening should be considered. It is recommended that the strengthened section fails after the internal steel yielding. To accomplish this condition the total design moment of the strengthened section, M_d, should be lower than the limit bending moment given by (5.61)

$$M_d \le M_{\lim} = 0.375 C_c d + \left(0.50 C_c - T_s\right)\left(h - d\right) \tag{5.61}$$

For the strengthened section, the increase in the height of the compression block, Δy, is calculated using equation (5.62). By incorporating this value into equation (5.63), the design value of the laminate tensile force, T_L, is obtained.

$$M_d = M_{u,0} + C_c \frac{\Delta y}{d}\left(h - y_0 - \frac{\Delta y}{2}\right) \tag{5.62}$$

$$T_L = C_c \frac{\Delta y}{d} \tag{5.63}$$

Finally, the laminate area necessary to strengthen the concrete section depends on the failure mode. The ultimate bending moment, M_u, and the ultimate increase in the height of the compression block, Δy_u, are given by equations (5.64) and (5.65) respectively.

$$M_u = M_{u,0} + C_c \frac{\Delta y_u}{d}\left(h - y_0 - \frac{\Delta y_u}{2}\right) \tag{5.64}$$

$$\Delta y_u = 0.8 \frac{\varepsilon_{cu}}{\varepsilon_{cu} + \min\left\{\varepsilon_{Lu}; \varepsilon_{L,pureflexure} = 2 s_{L0} / s_{cr}\right\}} h - y_0 \tag{5.65}$$

If the total design bending moment is lower than the ultimate bending moment ($M_d \leq M_u$), flexural failure may occur with the yielding of the steel reinforcement followed by the FRP rupture or by a pure flexure peeling failure. Therefore, the laminate area will be calculated by dividing the design value of the laminate tensile force by the ultimate laminate tensile stress, as shown in equation (5.66).

$$A_L = \frac{T_L}{E_L \min\left\{\varepsilon_{Lu}; \varepsilon_{L,pureflexure} = 2 s_{L0} / s_{cr}\right\}} \tag{5.66}$$

If the total design moment is higher than the ultimate bending moment ($M_d > M_u$), the flexural strength should be reached after the yielding of the tensile steel reinforcement, which is followed by the crushing of the concrete in the compression zone. Meanwhile, the FRP is intact. In this case, the laminate area depends on the value of the laminate strain, which is found by applying strain compatibility as a function of the ultimate compressive strength in the concrete (ε_{cu}).

$$A_L = \frac{T_L}{E_L \varepsilon_L} \tag{5.67}$$

$$\varepsilon_L = \varepsilon_{cu} \frac{h - x}{x} \tag{5.68}$$

Once the laminate area needed to strengthen the concrete section is found, it should be verified that no composite action is lost prior to the failure modes mentioned above. Composite action is lost when bond failure happens, that is, if the laminate peels-off due to the effect of cracks or due to stress concentration at the end of the laminate.

According to §5.2.4, if the shear force-bending moment at any section is under the curve defined in Figure 5.8, the externally reinforced concrete element will not fail due to the peeling effect generated between two cracks. Hence, the following design step will be based on the limit relationship between the shear force and the bending moment.

To avoid peeling failure due to the effect of cracks, the following iterative procedure should be performed. Firstly, the crack distance, s_{cr} is estimated by using, for example, the guidelines of the FIB Task Group 9.3 FRP (2001). Secondly, the pair (V_d, M_d) is plotted for each beam section. Thirdly, the steel yield bending moment, M_y, is determined through a moment-curvature analysis for the section strengthened with the laminate area required for flexural strengthening A_L. By using both data, s_{cr} and M_y, the simplified shear force-bending moment relationship is obtained. Then, if the pairs of design shear force and bending moment associated to each beam section are under the maximum shear force-bending moment relationship, the area required for flexural strengthening A_L will be enough to avoid peeling failure. On the contrary, if a pair of design shear force-bending moment values is over the peeling limit line, the laminate area required for flexural strengthening should be increased, and the peeling failure

should be checked again. The laminate area should be increased iteratively until the condition of being under the maximum shear force-bending moment limit is verified.

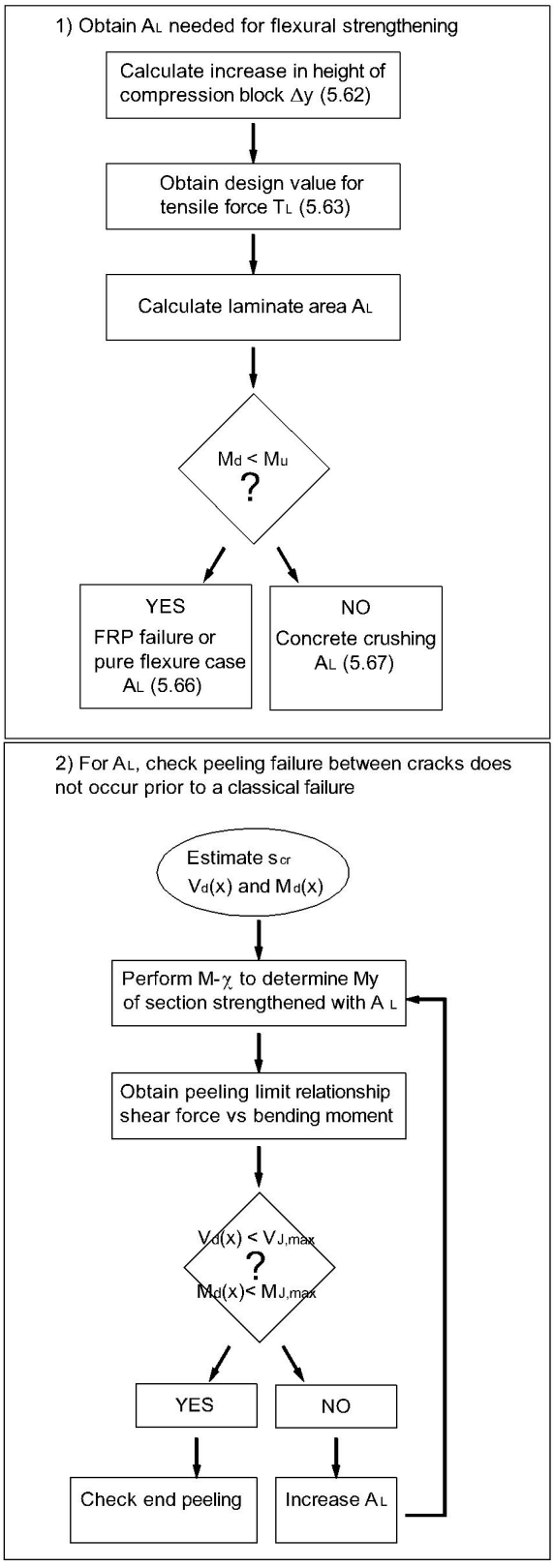

Figure 5.15. Design procedure (I).

Figure 5.15 represents schematically the design steps to determine the laminate area required for flexural strengthening and avoid peeling failure.

Once the laminate area is defined, the appearance of a peeling failure between the laminate end and the nearest crack will be checked by following the same procedure as described in §5.3. The section associated to the cracking moment under the design load defines the distance $L_{b,end}$. The laminate tensile force associated to the cracking moment is obtained through the moment-curvature analysis. This tensile force is compared to the maximum transferred force between the laminate end and the first crack. If the tensile force from the moment-curvature analysis is less than the theoretical maximum transferred force, the design procedure will be complete. If not, the laminate will locally debond between the first crack and the laminate end. Since this local debonding may or may not lead to complete laminate debonding, an additional verification should be performed. For this purpose, the element between the first two cracks should be checked. The laminate will completely peel-off if the local debonding propagates through the beam span. If the laminate tensile force in the most loaded crack is lower than the theoretical maximum transferred force at the laminate end for an element whose length is the crack distance, the debonding at the laminate will be local and the design procedure will end. If not, the laminate area will be increased and the beam element at the laminate end must be verified again. Figure 5.16 shows the flow chart related to the peeling verification at the laminate end.

Finally, as mentioned previously, both design and verification proposals depend on the maximum transferred force between cracks or at the laminate end. According to Chapter 4, the maximum transferred force is derived from the interfacial shear stress distribution. The interfacial normal stress distribution is not explicitly considered. However, the maximum transferred force depends on the fracture energy which represents the total concrete fracture and implicitly includes a component that depends on the interfacial normal stresses. Therefore, in a lab or field test, the total fracture energy is measured, and includes the energy that originates from the interfacial shear and normal stresses.

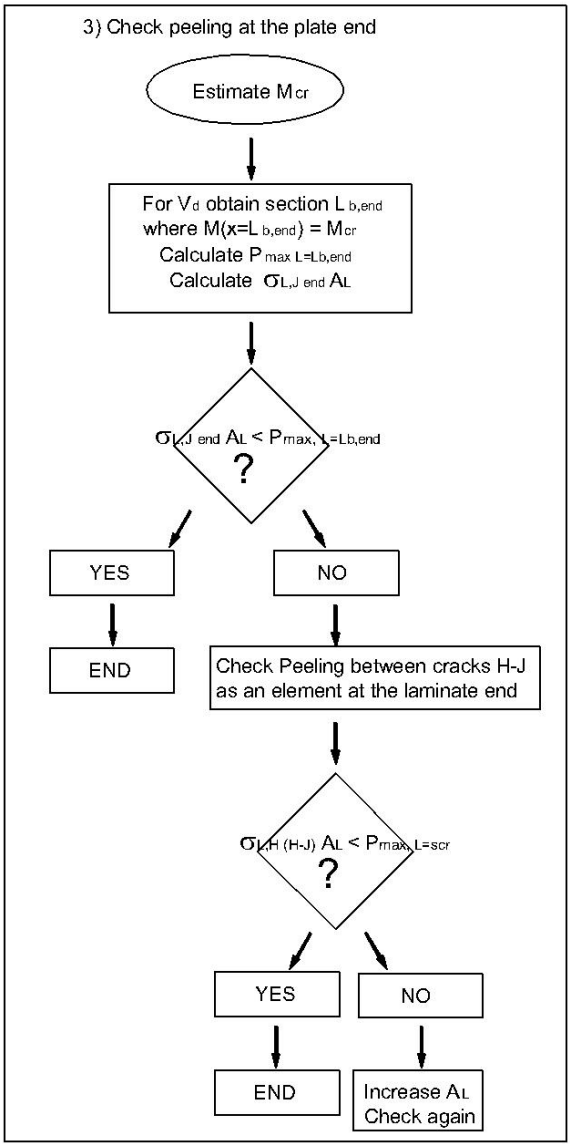

Figure 5.16. Design verification (II).

5.5. Application example of the proposed method

An application example is studied in this section, which deals with the design of an externally bonded laminate to strengthen a simply supported beam under uniform transverse loads.

The analyzed beam has a single span of 4.0 *m* and a cross-section of 0.40 x 0.25 *m* with an existing internal steel reinforcement of 3ϕ20. The beam was cast in a 30 MPa concrete strength. The design bending moment at midspan is 72.0 *kNm*. A change in the use of the structure implies an increment of 12.5 *kN/m* on the live load. The increment of load implies an increase of 40.0 *kNm* on the bending moment at midspan, so the total design moment at midspan becomes 112.0 *kNm*. The ultimate bending moment of the unstrengthened section with its internal steel reinforcement, $M_{u,0}$, is 69.6 *kNm*. As the total design moment is higher than the ultimate bending moment, it is necessary to

strengthen the beam element. In order to do so, an externally bonded FRP laminate will be bonded to the beam soffit. Pultruded laminates whose modulus of elasticity is 150 *GPa* are employed in this example.

The laminate area needed for flexural strengthening is obtained by following the procedure described in the previous section. The design value of the laminate tensile force, T_L, is obtained as 247.1 *kN*. Since the design bending moment of the strengthened section at midspan, M_d, is higher than the ultimate bending moment, failure will occur when the concrete crushes in the compression zone. Therefore, the laminate area depends on the value of the laminate strain associated to the ultimate strain in the concrete ε_{cu}. Since the laminate area needed for flexural strengthening is 270 mm^2, it was decided to bond two pultruded laminates of 100 x 1.4 *mm*.

The laminate area required to strengthen the concrete section should be the area necessary not only for flexural capacity but also the area which avoids the premature peeling failure between cracks and at the laminate end. Therefore, peeling failure will be checked first between cracks, assuming a laminate area equal to that required for flexural strengthening, 280 mm^2. For this purpose, the crack distance is estimated as 145 mm according to the guidelines of FIB Task Group 9.3 FRP (2001). Through moment-curvature analysis, the yield bending moment of the reinforced cross-section is found to be M_y = 95.3 *kNm*. By knowing the concrete's properties, the maximum shear stress of the bond-slip relationship, τ_{LM}, can be obtained as 2.36 *MPa*. The slip associated to the maximum shear stress, s_{LM}, and the maximum sliding, s_{L0} can be calculated using equations (3.119) and (3.122) as 0.013 and 0.753 mm, respectively. Through this data, the next step consists of calculating the maximum shear force-bending moment relationship that avoids peeling failure, as shown in Figure 5.17. Afterwards, the relationship between the design shear force V_d and the design bending moment M_d is plotted for each section between the support and midspan. Since the complete plotted line $V_d(x) - M_d(x)$ is under the peeling limit relationship (see Figure 5.17), the laminate area 2 x 100 x 1.40 *mm* is enough to avoid the peeling effect between cracks. If this had not been accomplished, the laminate area would have been increased and this procedure would have been performed again.

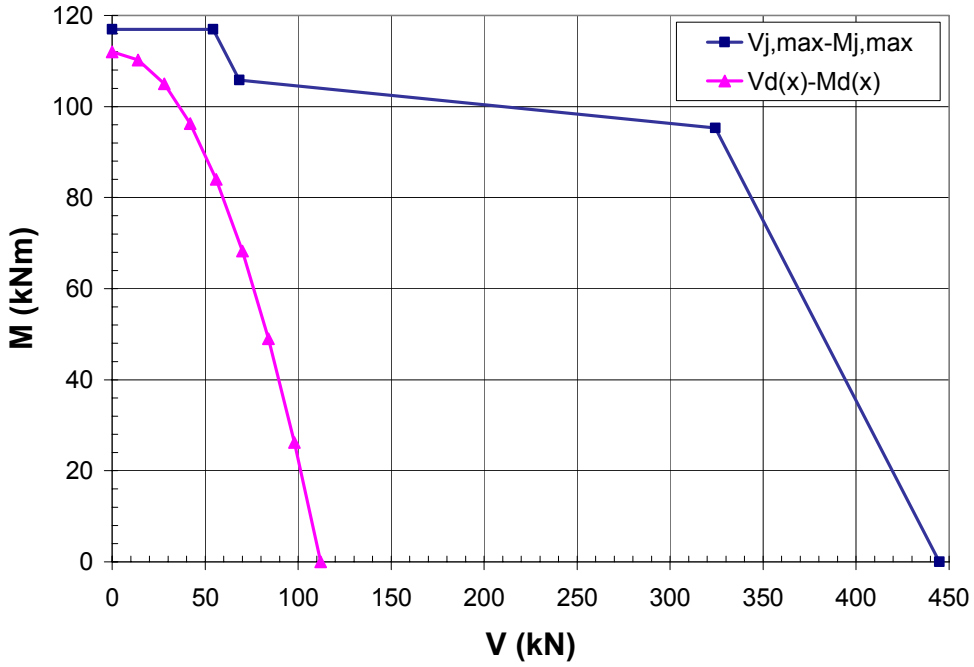

Figure 5.17. Verification of peeling failure between cracks in a beam under uniform load.

At this point, peeling failure at the laminate end should be checked. The cracking moment according to the FIB Task Group 9.3 is equal to 19.8 *kNm*. From the design bending moment law, the first crack appears at a distance of 217 *mm* from the support. By assuming an unbonded length of 50 *mm*, the distance between the laminate end and the nearest crack is 167 *mm*. The maximum transferred force along this distance is 91.7 *kN* when considering the concrete contribution in tension. The design value of the tensile force at the cracking moment location is 23.3 *kN*, which is less than the maximum transferred force. Therefore, peeling failure will first initiate between cracks rather than at the laminate end.

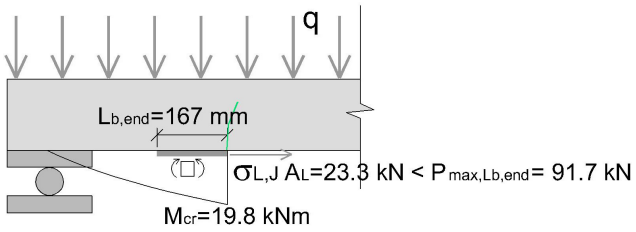

Figure 5.18. Verification of peeling at the laminate end in a beam under uniform load.

This is an example of a simply supported beam under a uniform load configuration. With regards to peeling failure between cracks, the demand of the shear force-bending moment in a three-point bending configuration is higher than in a uniform load case with the same bending moment at midspan, as observed in Figure 5.19. By increasing the applied load in both cases, peeling will initiate in the three-point bending configuration when the bending moment reaches 114.0 *kNm*. For the uniform load case, the concrete will crush at 117.0 *kNm* before the laminate peels off (see Figure 5.20). This observation suggests that in real cases where structures are under uniform load configurations, the technique of externally bonding FRP laminates is not as unsafe as lab tests under 3 or 4-point bending configurations suggest.

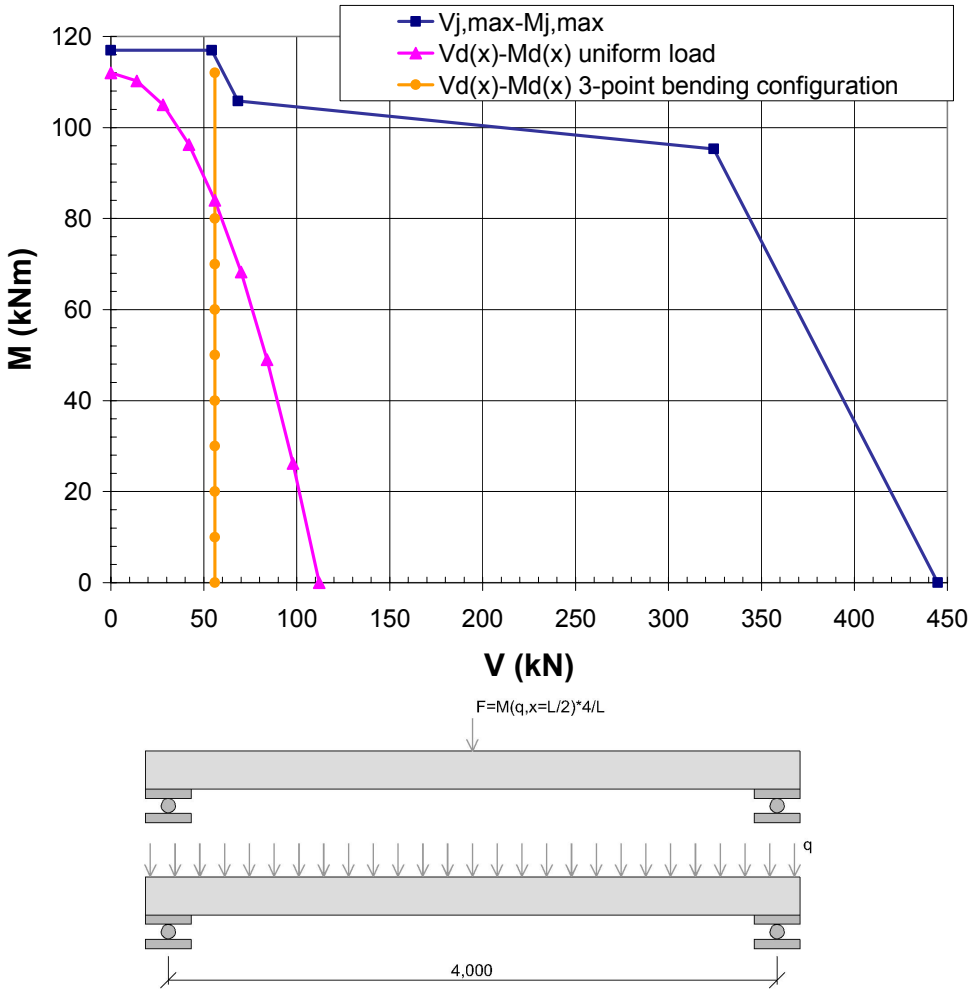

Figure 5.19. Equivalent 3-point bending configuration case.

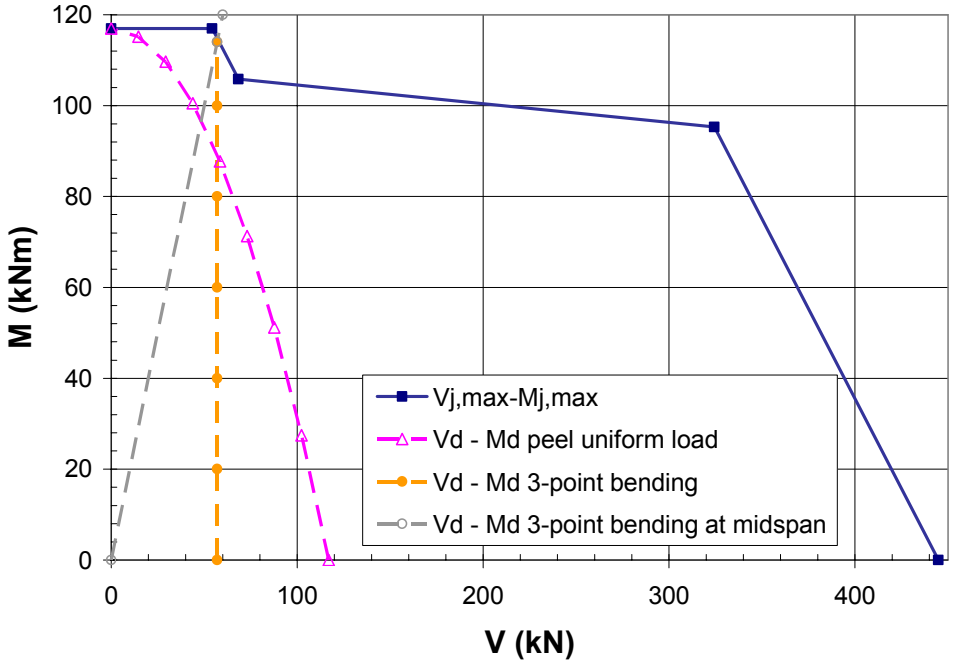

Figure 5.20. Failure for the uniform load and the 3-point bending configuration case.

5.6. Verification of the proposed method with the experimental database

The proposed design/verification method is checked in this section by using the experimental database of flexural tests presented in Chapter 2. The database consists of 587 flexural tests from which only those well-known externally strengthened beams without external anchorages that failed by premature laminate debonding were chosen (300 tests). From the peeling database, a total of 64 tests were excluded: 38 tests because no FRP laminate was bonded to their soffit, 1 test because no internal steel was used, 1 test with slot-applied laminates, 1 test strengthened by using both a wet lay-up and a pultruded laminate, 7 tests that were cast in high-strength concrete, and 18 tests because the ultimate bending moment obtained from the moment-curvature analysis was lower than the experimental value. Hence, a total of 234 specimens from the database have been studied.

First, a moment-curvature analysis of each strengthened element has been performed to find the yield bending moment and the ultimate bending moment due to concrete crushing or FRP rupture. Then, the average crack distance has been calculated according to the guidelines of the FIB Task Group 9.3 (2001). The model parameters τ_{LM}, s_{LM}, and s_{L0} are calculated by using the geometry and material data. Some other constants such as Ω_2 are also obtained from the model parameters.

All analyzed beams were tested in a three or four-point bending configuration. Under this load configuration, the shear force is constant along the shear span and the maximum bending moment is reached at the load application point. Since no crack distribution is available in the majority of assembled tests, the verification procedure has been applied at the load application point.

The verification process described in §5.3 consists of comparing the ultimate shear force obtained during the test at the studied section, V_{exp}, to the intersection of the experimental shear force-bending moment relationship with the theoretical limit of maximum shear force that prevents peeling failure. Since the committed error is negligible, the simplified maximum shear force-bending moment relationship, which was defined in §5.2.4, has been used for this purpose.

For each key point of the simplified maximum shear force vs. bending moment relationship, the arc tangent of the quotient between the bending moment and the shear force is calculated as $\theta^{(i)}$ (see equation (5.48)). Due to the load configuration, the angle associated to the experimental failure load, θ_{exp}, is equal to the arc tangent of the shear span. The experimental failure angle θ_{exp} is compared to the key point angles, $\theta^{(i)}$. Such a comparison gives an idea of the situation at failure, in other words, whether the internal steel has yielded or not in crack J or/and crack I. In addition, it helps to identify the intersection point of the experimental line given by θ_{exp} with the shear force limit line. The intersection point, calculated as equation (5.51), gives the maximum shear force that can be reached before peeling initiates between cracks under the load application point.

An additional verification should be performed at the laminate end to check if the laminate has previously failed at this location. This verification is performed according

to §5.3. If a local failure occurs between the laminate end and the first crack, the element between the first two cracks will be checked. In case the tensile force in the second crack is higher than the maximum transferred force along the crack distance, the predicted maximum shear force V_{cracks} is readjusted to V_{end}.

The lowest value, V_{pred}, of either the shear force associated to peeling at the load application point, V_{cracks} or the shear force associated to peeling at the laminate end, V_{end}, is the maximum shear force that can be attained before a brittle failure involving laminate debonding.

The ratio V_{exp}/V_{pred} indicates the approximation of the theoretical formulae to the experimental results. Ratios higher than 1.0 represent a conservative theoretical formulation which underestimates the response of the strengthened member. This is the case for 208 out of the 234 studied specimens.

For the total number of beams that showed peeling failure, the ratio between the experimental and theoretical maximum shear force has a mean value of 1.26 with a standard deviation of 0.33. The median of 1.19, similar to the mean, gives an idea of the homogeneity of the sample. The coefficient of variation, known as the ratio between the mean and the standard deviation, is 26%, which is lower than those obtained from the better performing models analyzed in §2.4. The proximity to 1.0 of both one-percentile (0.73) and ninety-nine percentile (2.20) shows the good performance of the model in terms of safety.

Peeling failure is theoretically initiated due to the effect of cracks in 208 tests out of the 234 analyzed tests. 23 out of these 208 tests theoretically showed local debonding at the laminate end. This local debonding is limited by the first crack nearest to the laminate end, and does not imply a complete laminate debonding which theoretically initiates due to the effect of cracks. The statistical performance of these 23 tests is similar to the rest of the beams that failed near flexural or shear cracks. In the remaining 26 out of the 234 analyzed tests, failure is theoretically initiated at the plate end and propagates towards midspan. The shear force that prevents peeling failure between cracks is readjusted to prevent peeling failure at the laminate end. This readjustment shows a similar scatter with a coefficient of variation equal to the coefficient obtained from peeling initiated near cracks.

Table 5.1. Experimental-to-theoretical ratios for the verification proposal given in §5.3.

	Ratio	#	Min	Mean	Max	Med	Std dev	COV	$(X_{exp}/X_u)_{1\%}$	$(X_{exp}/X_u)_{99\%}$
(1)	(2)	(3)	(4)	(5)	(6)	(7)	(8)	(9)	(10)	(11)
Total peeling failure tests	V_{exp}/V_{pred}	234	0.67	1.26	2.65	1.19	0.33	0.26	0.73	2.20
Th. peeling failure cracks		208	0.67	1.23	2.65	1.16	0.30	0.25	0.69	2.09
Th. end peeling failure tests		26	0.84	1.55	2.26	1.48	0.39	0.25	0.80	2.56

(*) Th.: Theoretical

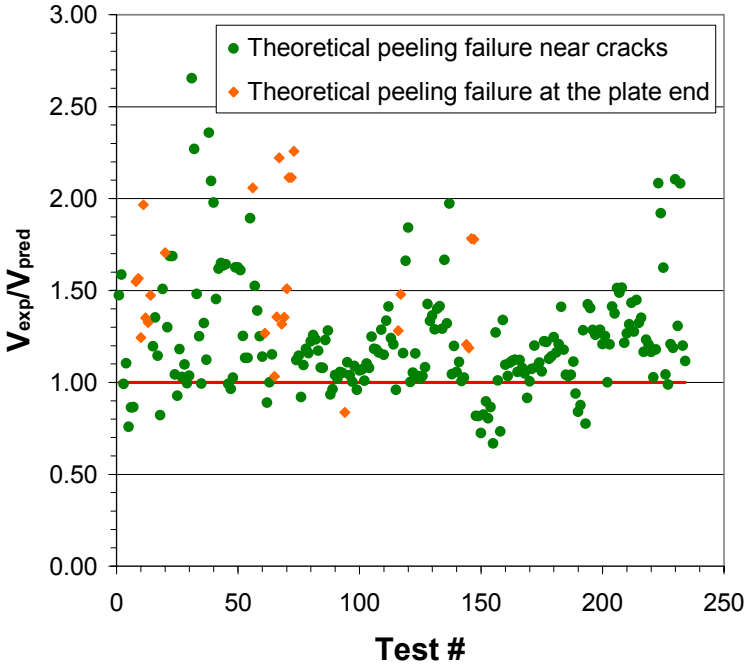

Figure 5.21. Ratio between experimental and predicted maximum shear force.

In Figure 5.21, the ratio V_{exp}/V_{pred} is plotted for all the analyzed tests that failed due to peeling. A distinction between theoretical peeling initiation points has been made. As observed, the ratios for the vast majority of tests that theoretically failed due to peeling caused by the effect of cracks fall in the range between 1.0 and 1.5. A large scatter is observed when peeling theoretically initiates at the laminate end. Regardless of the peeling initiation point, only a small number of tests show a non-conservative ratio of less than 1.0.

The "Demerit Points Classification" of Collins (2001), described in Chapter 2, is applied to this model by assigning a mark called "Demerit Point" to each range of the ratios V_{exp}/V_{pred}. As observed in Table 5.2, the highest percentage of ratios (62.4%) is in the range between 0.85 and 1.30 which corresponds to appropriate safety. In addition, the range between 1.30 and 2.00, which is conservative, is the second largest, with a percentage of 27.3%. There are not tests in a dangerous or extremely dangerous range. A percentage of 5.1% is associated to a low safety level. With the exception of one specimen whose ratio is 0.67, the low safety level percentage corresponds to tests which have ratios between 0.76 and 0.84, which are almost close to an appropriate safety level.

Table 5.2 and Figure 5.22 separately analyze the demerit points score associated to theoretical peeling failure that initiates near flexural or shear cracks, and at the laminate end. For tests where peeling initiates near flexural or shear cracks, the percentage associated to an appropriate safety level is higher than for peeling in general. In addition, the percentage of tests in the conservative or extremely conservative ranges is lower than in the general case. As a consequence, the score of demerit points is lower than for peeling in general. The degree of conservativeness shown by the model is to a great extent due to the reduction of the theoretical maximum shear force for the 26 tests that theoretically failed at the laminate end. Here, the largest percentage of ratios

(53.8%) is in the conservative range of safety, followed by 23.1% which are in the appropriate safety range.

Table 5.2. Demerit point classification for beams failing by laminate peeling-off.

	Ratio	<0.50	0.50-0.65	0.65-0.85	0.85-1.30	1.30-2.00	>2.00	Total Demerit Points
Classification (*)		E.D.	D.	L.S.	A.S.	C.	E.C.	
Demerit Point		10	5	2	0	1	2	
Total peeling failure tests	V_{exp}/V_{pred}	0.00	0.00	5.13	62.39	27.35	5.13	48
Th. peeling due to cracks		0.00	0.00	5.29	67.31	24.04	3.37	41
Th. peeling at the plate end		0.00	0.00	3.85	23.08	53.85	19.23	100

(*) E.D.: Extremely dangerous; D.: Dangerous; L.S.: Low safety; A.S.: Appropiate safety; C.: Conservative; E.C.: Extremely conservative

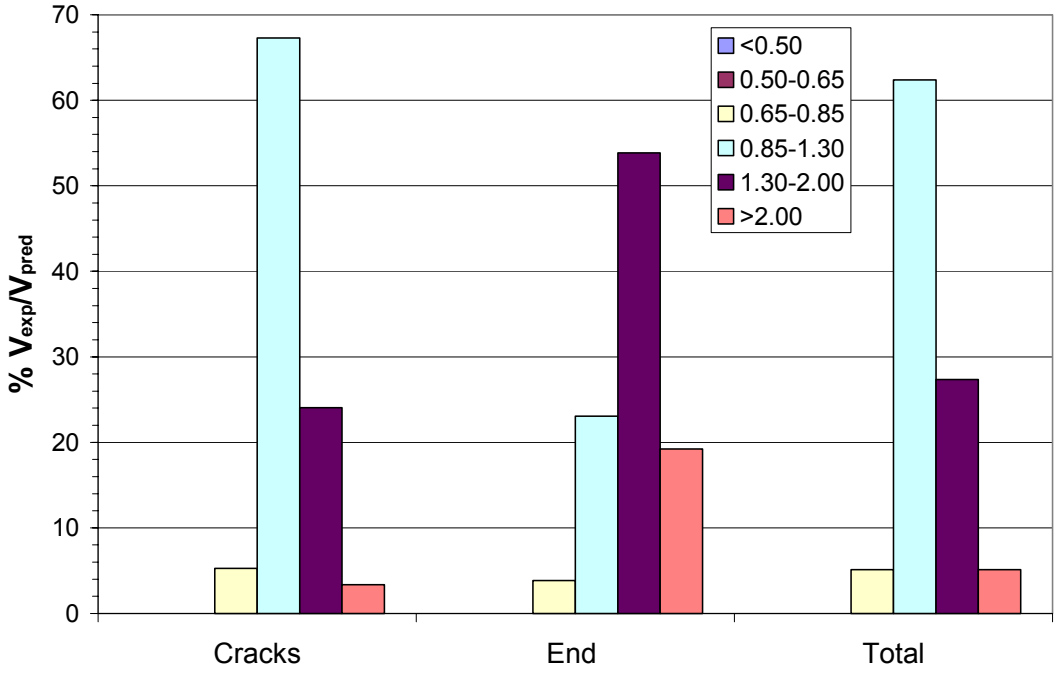

Figure 5.22. Percentages of ratios included in each range of the Demerit Points Classification.

The verification proposal presented in this Chapter is analyzed at this point by comparing the statistical results obtained when classifying specimens by their observed premature peeling failure mode. As shown in Table 5.3, specimens that were reported to fail by peeling initiated near flexural or shear cracks (184 tests) show a statistical performance similar to the total number of peeling tests (234 tests), with an almost identical mean, median and coefficient of variation. In theory, the laminate end locally debonded in 4 out of the 184 tests. As mentioned, this theoretical local debonding does not imply that a complete laminate peeling-off will initiate at this location. According to Table 5.3, the verification proposal showed a larger scatter for tests where peeling failure was observed due to a high stress concentration at the laminate end. Statistical results for plate end shear failure tests show a slightly more conservative mean value and a smaller scatter because of the small number of tests (13 tests). For the same reason, the developed model does not fit well with the non-symmetrical normal distribution developed by Collins (2001), as shown by the negative one-percentile

derived according to equation (2.55) of Chapter 2. As shown in Figure 5.23, almost all ratios for plate end shear failure tests fall between 1.0 and 1.5.

Table 5.3. Experimental-to-theoretical ratios distinguishing the observed peeling failure mode.

	Ratio	#	Min	Mean	Max	Med	Std Dev	COV	$(X_{exp}/X_u)_{1\%}$	$(X_{exp}/X_u)_{99\%}$
(1)	(2)	(3)	(4)	(5)	(6)	(7)	(8)	(9)	(10)	(11)
Total peeling failure tests	V_{exp}/V_{pred}	234	0.67	1.26	2.65	1.19	0.33	0.26	0.73	2.20
Peeling tests due to cracks		184	0.73	1.24	2.36	1.17	0.30	0.24	0.71	2.07
End peeling failure tests		37	0.67	1.36	2.65	1.25	0.45	0.33	0.74	2.74
Plate end shear failure tests		13	0.89	1.27	1.71	1.29	0.22	0.18	0.94	2.02

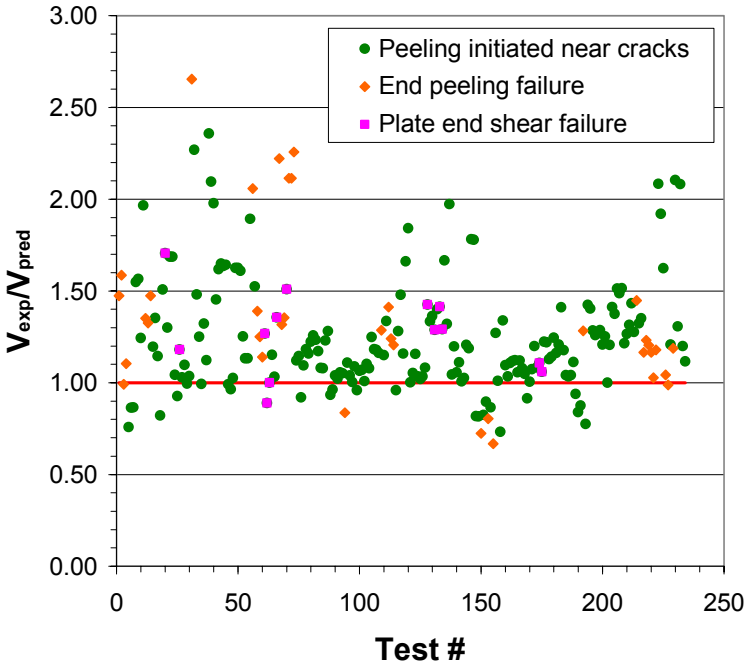

Figure 5.23. Ratio between experimental and predicted shear force for the observed failure modes.

As previously mentioned, the Demerit Points Classification of Collins gives a score of 48 for peeling failure in general. This score is reduced to 42 when studying peeling failure initiated near cracks. When filtering this type of peeling failure, the total number of demerit points is still lower than the score obtained by the existing models. The total demerit points observed for end peeling failure tests is 81. This fact is explained by the percentage of tests in the extremely conservative and low safety range. For plate end shear failure tests, the score decreases to 38 because all ratios belong to an appropriate or a conservative range of safety. Table 5.4 does not report plate end shear specimens below or in low safety ranges.

Table 5.4. Demerit Points Classification for the verification proposal of §5.3.

	Ratio	<0.50	0.50-0.65	0.65-0.85	0.85-1.30	1.30-2.00	>2.00	Total Demerit Points
Classification (*)		E.D.	D.	L.S.	A.S.	C.	E.C.	
Demerit Point		10	5	2	0	1	2	
Total peeling failure tests	V_{exp}/V_{pred}	0.00	0.00	5.13	62.39	27.35	5.13	48
Peeling tests due to cracks		0.00	0.00	4.35	65.76	26.63	3.26	42
End peeling failure tests		0.00	0.00	10.81	45.95	27.03	16.22	81
Plate end shear failure tests		0.00	0.00	0.00	61.54	38.46	0.00	38

(*) E.D.: Extremely dangerous; D.: Dangerous; L.S.: Low safety; A.S.: Appropiate safety; C.: Conservative; E.C.: Extremely conservative

In some cases, the observed mode of failure does not match with the theoretical prediction. Therefore, an identical statistical analysis is now performed for all tests but with a distinction between both theoretical and observed failure initiation point. Table 5.5 summarizes the ratios for those tests that theoretically failed near the load application point. This peeling failure mode was confirmed by the proposal in 173 out of the 184 where failure was reported to be induced by the cracks' effects. The remaining 11 specimens theoretically failed first at the laminate end. Even though failure was reported to be due to the effect of cracks in these 11 tests, it should not be forgotten that it is always difficult to identify the origin of peeling failure because of its brittleness and its propagation speed. This fact was also observed during the experimental program performed by the author. The total number of tests (15) that showed a theoretical local debonding at the plate end failed in both theory and practice due to the effect of cracks. Peeling theoretically initiates near the load application point in 26 tests (out of 37) that experimentally failed at the plate end. The statistical performance of these tests is similar to the general trends for theoretical peeling due to cracks with a slightly lower mean, median and coefficient of variation. Curiously, almost all the tests (9 out of 13) that were reported to fail by a shear crack at the laminate end theoretically failed due to flexural or shear cracks near the load application point.

Table 5.5. Experimental-to-theoretical ratios for tests that in theory failed by peeling near cracks.

	Ratio	#	Min	Mean	Max	Med	Std dev	COV	$(X_{exp}/X_u)_{1\%}$	$(X_{exp}/X_u)_{99\%}$
(1)	(2)	(3)	(4)	(5)	(6)	(7)	(8)	(9)	(10)	(11)
Th. peeling due to cracks	V_{exp}/V_{pred}	208	0.67	1.23	2.65	1.16	0.30	0.25	0.69	2.09
Peeling tests due to cracks		173	0.73	1.23	2.36	1.16	0.30	0.24	0.69	2.03
End peeling failure tests		26	0.67	1.23	2.65	1.20	0.36	0.30	0.62	2.23
Plate end shear failure tests		9	0.89	1.18	1.43	1.18	0.19	0.16	0.77	1.59

Table 5.6 shows the experimental-to-theoretical ratios for tests that theoretically failed due to end peeling. The model confirms the observed mode of failure in 11 out of the 26 tests that theoretically failed by end peeling. In addition, in only 4 out of all tests that failed by plate end shear failure (13), peeling theoretically initiated between the laminate end and the nearest crack. In general, the developed model is more conservative for peeling initiated at the plate end than for peeling in general. The data used in both Table 5.5 and Table 5.6 are gathered in Figure 5.24.

Table 5.6. Experimental-to-theoretical ratios for tests that in theory failed by end peeling.

	Ratio	#	Min	Mean	Max	Med	Std dev	COV	$(X_{exp}/X_u)_{1\%}$	$(X_{exp}/X_u)_{99\%}$
(1)	(2)	(3)	(4)	(5)	(6)	(7)	(8)	(9)	(10)	(11)
Th. peeling at the plate end	V_{exp}/V_{pred}	26	0.84	1.46	2.26	1.48	0.39	0.25	0.80	2.56
Peeling tests due to cracks		11	1.03	1.43	1.97	1.48	0.30	0.20	1.15	2.78
End peeling failure tests		11	0.84	1.67	2.26	1.47	0.49	0.29	0.99	3.54
Plate end shear failure tests		4	1.27	1.46	1.71	1.43	0.19	0.13	1.13	2.43

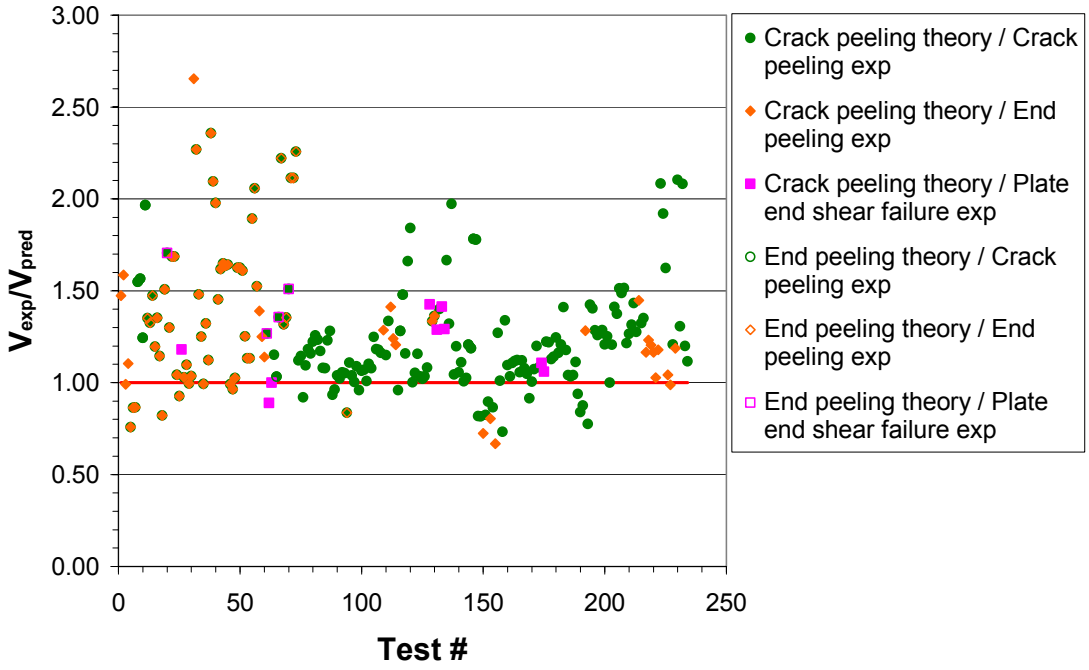

Figure 5.24. Ratio between experimental and predicted shear force for the theoretical and observed failure modes.

Both Table 5.7 and Table 5.8 summarize the score of Demerit Points after classifying the theoretical and observed failure mode. All tests that failed in theory due to the effect of cracks near the load application point obtained similar scores in the range of 41 and 54, with the exception of those tests that failed due to a shear crack at the laminate end, having a lower score of 22 (see Table 5.7). The small number of tests that failed due to a shear crack at the laminate end does not have a significant influence in the total score of demerit points.

Table 5.7. Demerit Points Classification for tests that failed in theory near cracks.

	Ratio	<0.50	0.50-0.65	0.65-0.85	0.85-1.30	1.30-2.00	>2.00	Total Demerit Points
Classification (*)		E.D.	D.	L.S.	A.S.	C.	E.C.	
Demerit Point		10	5	2	0	1	2	
Th peeling due to cracks	V_{exp}/V_{pred}	0.00	0.00	5.29	67.31	24.04	3.37	41
Peeling tests due to cracks		0.00	0.00	4.62	67.05	24.86	3.47	41
End peeling failure tests		0.00	0.00	11.54	65.38	19.23	3.85	54
Plate end shear failure tests		0.00	0.00	0.00	77.78	22.22	0.00	22

(*) E.D.: Extremely dangerous; D.: Dangerous; L.S.: Low safety; A.S.: Appropiate safety; C.: Conservative; E.C.: Extremely conservative

In relation to theoretical peeling plate end failures (Table 5.8), the higher score is caused by tests that failed in both theory and practice by end peeling. The score for the 11 tests where failure was observed near cracks is slightly larger (54) than those in the same category found in Table 5.7 (41). The demerit points obtained by plate end shear failure tests do not have a significant meaning because only four beams belong to this group.

Table 5.8. Demerit Points Classification for tests that failed in theory at the plate end.

	Ratio	<0.50	0.50-0.65	0.65-0.85	0.85-1.30	1.30-2.00	>2.00	Total Demerit Points
Classification (*)		E.D.	D.	L.S.	A.S.	C.	E.C.	
Demerit Point		10	5	2	0	1	2	
Th. peeling at the plate end	V_{exp}/V_{pred}	0.00	0.00	3.85	23.08	53.85	19.23	100
Peeling tests due to cracks		0.00	0.00	0.00	45.45	54.55	0.00	54
End peeling failure tests		0.00	0.00	9.09	0.00	45.45	45.45	154
Plate end shear failure tests		0.00	0.00	0.00	25.00	75.00	0.00	75

(*) E.D.: Extremely dangerous; D.: Dangerous; L.S.: Low safety; A.S.: Appropiate safety; C.: Conservative; E.C.: Extremely conservative

In view of the fact that some intermediate cracks appeared after service load during the Experimental Program described in Chapter 2, the influence of the average crack distance is studied. The previous analysis has been performed by assuming an average crack distance calculated according the guidelines of the FIB Task Group 9.3 which took into account the effect of the laminate. In general, this value is slightly larger than the crack distance obtained by using the Spanish Concrete Code (EHE, 1999). Both values in addition to that developed by Raoof et al. (1997) and that of the Eurocode 2 (draft of 2003) are compared. The draft of the Eurocode 2 suggests a more realistic formula of the crack distance that depends on the concrete cover. Since this parameter is known for almost all tests of the database, the crack distance according to the draft of the Eurocode 2 has been used in this study instead of the current regulation.

In order to consider the intermediate cracks that appeared at high load levels according to some references, a crack distance equal to half of the value calculated according the guidelines of the FIB Task Group 9.3 has also been studied.

As shown in Table 5.9, the statistical performance of the varying crack distances under study is similar in terms of mean, median and coefficient of variation. The larger scatter is observed for the crack distance defined by Raoof et al. In terms of safety, the crack distance of the FIB Task Group 9.3 and the crack distance of the Eurocode 2 give the better combination of the highest one-percentile and the lowest ninety-nine percentile. Results according to the Spanish Concrete Code are similar with a slightly higher ninety-nine percentile. By considering half of the FIB Task Group 9.3 crack distance, results scarcely vary in terms of mean and median. The main difference is given by a slightly larger scatter.

Table 5.9. Experimental-to-theoretical ratios for different crack distances.

Crack distance	Ratio	#	Min	Mean	Max	Med	Std Dev	COV	$(X_{exp}/X_u)_{1\%}$	$(X_{exp}/X_u)_{99\%}$
s_{cr}, FIB	V_{exp}/V_{pred}	234	0.67	1.26	2.65	1.19	0.33	0.26	0.73	2.20
s_{cr}, EHE			0.67	1.28	3.86	1.18	0.38	0.30	0.74	2.41
s_{cr}, EC-2 (draft)			0.69	1.27	3.07	1.20	0.34	0.27	0.74	2.24
s_{cr}, Raoof et al. (1997)			0.57	1.17	6.90	1.17	0.69	0.51	0.66	3.49
s_{cr}, FIB/2			0.59	1.30	3.23	1.16	0.45	0.35	0.69	2.63

The scores obtained by the Demerit Points classification range from 47 to 66 (see Table 5.10), which are always lower than those obtained by the better performing models given in Chapter 2. The percentages of tests in each safety level do not differ too much. The same trend is followed by all values of the crack distance. The similar scores of Demerit Points and the similar statistical results show that the influence of the crack distance is not very significant. The lowest score is obtained by both the crack distance of the FIB Task Group 9.3 and the crack distance of the Eurocode 2 draft. However, since the Eurocode 2 draft does not consider the influence of the laminate on the crack distance calculation, the author recommends the application of the formula of the FIB Task Group 9.3 FRP. It has been observed on the analysis that depending of the specimen's properties, one of those two better performing guidelines gives the highest value for the crack distance.

Table 5.10. Demerit Points Classification for different crack distances.

Peeling tests due to cracks	Ratio	<0.50	0.50-0.65	0.65-0.85	0.85-1.30	1.30-2.00	>2.00	Total Demerit Points
Classification (*)		E.D.	D.	L.S.	A.S.	C.	E.C.	
Demerit Point		10	5	2	0	1	2	
s_{cr}, FIB	V_{exp}/V_{pred}	0.00	0.00	5.13	62.39	27.35	5.13	48
s_{cr}, EHE		0.00	0.00	5.56	59.40	28.63	6.41	53
s_{cr}, EC-2 (draft)		0.00	0.00	4.31	62.07	28.88	4.74	47
s_{cr}, Raoof et al. (1997)		0.00	2.14	3.85	56.41	27.78	9.83	66
s_{cr}, FIB/2		0.00	0.85	4.70	59.83	26.07	8.55	57

(*) E.D.: Extremely dangerous; D.: Dangerous; L.S.: Low safety; A.S.: Appropiate safety; C.: Conservative; E.C.: Extremely conservative

A characteristic lower bound of the ratio V_{exp}/V_{pred} can be obtained by the five percentile. When calculating the crack distance according to the Task Group 9.3 FRP, 95% of tests, that is the five percentile $(V_{exp}/V_{pred})_{5\%}$, show an experimental ultimate shear force higher than 0.87 times the predicted value. Then, a characteristic lower bound of 0.87 times the median maximum shear load is advised by the author. As a consequence, to achieve a safe design, the characteristic value of the maximum shear force will be obtained by be dividing the prediction given by the current proposal by a factor of 1.15.

From the statistical analysis performed in Chapter 2, the more robust performing models in predicting peeling failure were: the truss analogy based model of Colotti and Spadea (2001), the shear based capacity model of Ali et al. (2001) and the lower prediction of the concrete tooth model of Raoof et al. (1997, 2000a, 2000b, 2001). Figure 5.25 shows a comparison between the three existing models and the verification procedure presented in this Chapter in percentage terms of X_{exp}/X_u that are associated to different safety levels. The best performing model is the one developed by the author in this

Chapter, with the highest percentage of tests in the ranges of appropriate and conservative safety, and with only 5.13 percent of tests in a low safety range. The second better performing model is that of Ali et al. which has a slightly lower percentage of tests in the appropriate safety range, a lower percentage of conservative tests and a higher percentage of specimens in the low and dangerous safety ranges. The most conservative model is that of Colotti and Spadea. These trends are also reflected in the Demerit Points Classification (see Figure 5.26).

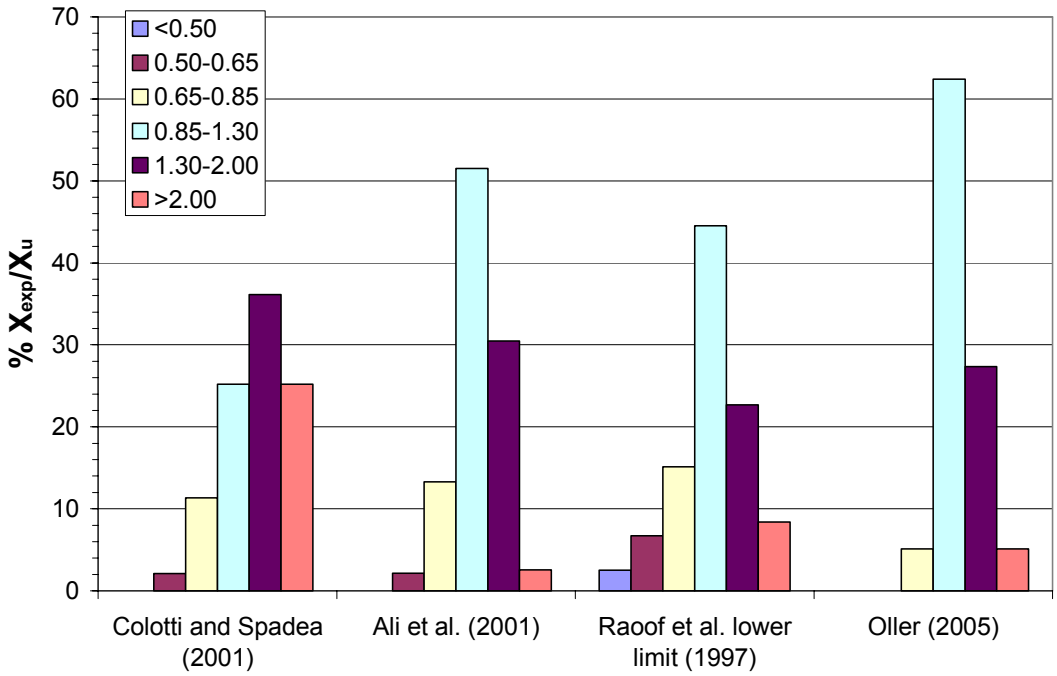

Figure 5.25. Comparison of the statistically better performing models.

The Demerit Point Classification gives a score of 48 to the proposal of verification described in §5.3. This value is much lower than the score obtained by the existing models described in Chapter 2 when analyzing the same number of tests: Ali et al. scored 73; Colotti and Spadea scored 120; and finally, Raoof et al., at 129.

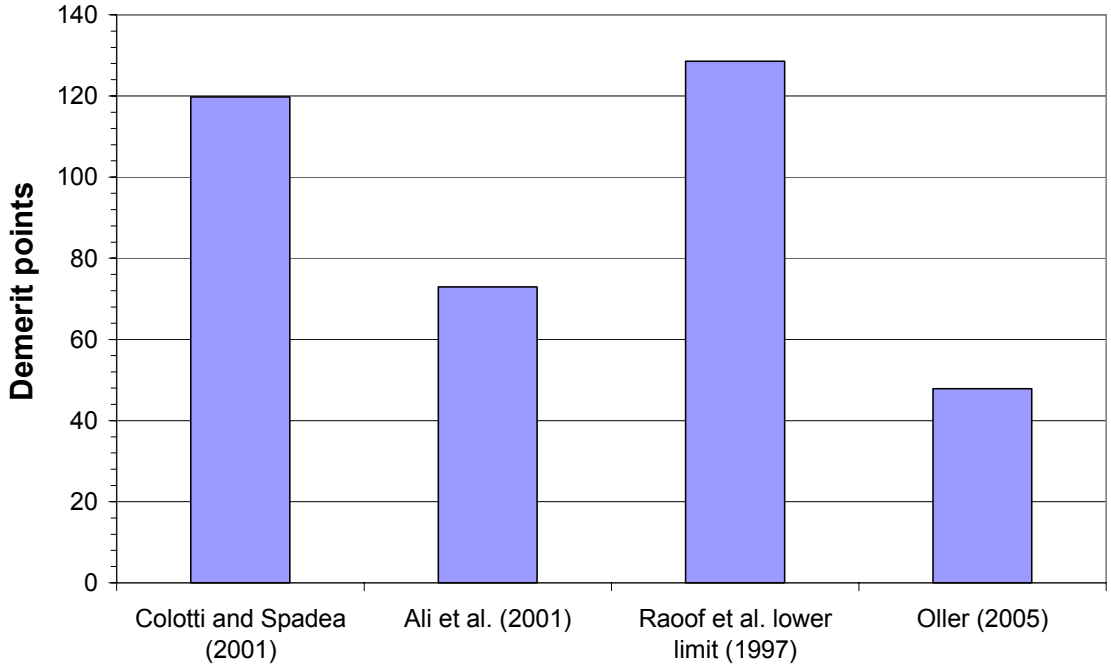

Figure 5.26. Better scored models by using the Demerit Point Classification.

Table 5.11 compares the demerit points obtained by the existing models of Colotti and Spadea, Ali et al., Raoof et al. and the current proposal when studying those tests that failed due to peeling in general.

Table 5.11. Demerit Points Classification for peeling failure in general.

Peeling tests due to cracks	Ratio	<0.50	0.50-0.65	0.65-0.85	0.85-1.30	1.30-2.00	>2.00	Total Demerit Points
Classification (*)		E.D.	D.	L.S.	A.S.	C.	E.C.	
Demerit Point		10	5	2	0	1	2	
Colotti and Spadea (2001)	V_{exp}/V_{pred}	0.00	2.10	11.34	25.21	36.13	25.21	120
Ali et al. (2001)		0.00	2.15	12.88	51.50	30.90	2.58	73
Raoof et al. (1997)		2.52	7.14	15.13	47.48	19.75	7.98	129
Oller (2005)		0.00	0.00	5.13	62.39	27.35	5.13	48

(*) E.D.: Extremely dangerous; D.: Dangerous; L.S.: Low safety; A.S.: Appropiate safety; C.: Conservative; E.C.: Extremely conservative

Since the models of Colotti and Spadea, Ali et al., and Raoof et al. were developed to prevent peeling failure due to either flexural or shear cracks, only those tests where peeling was observed to initiate near cracks are now studied. The better performing model according to Collins' classification is found to be the current proposal (with a total score in demerit points of 41) followed distantly by Ali et al.'s model (score of 74). In addition, for experimental end peeling failures, the current model performed better than the linear elastic models combined with a failure criterion. The current model is slightly conservative for these cases.

From the proposal verification using the bending test database, some conclusions are summarized as follows:

1) The developed verification procedure shows good statistical performance in terms of a safe mean and median and a low coefficient of variation. This is also shown by the proximity of both the one percentile and the ninety-nine percentile to 1.0.
2) In terms of Demerit Points, the total score when studying all tests that failed by peeling is 48, a score lower than those obtained by the existing models.
3) The proposal performs better for those tests that theoretically failed due to the effect of cracks. For theoretical end peeling failures, the proposal shows a larger scatter and a higher degree of conservativeness.
4) The model correctly predicts the peeling failure mode in 173 out of the 184 tests that failed by peeling due to the effects of cracks. In addition, the model predicts accurately peeling failure at the laminate end in 11 out of 37 tests.
5) The influence of the crack distance is not very significant. The most accurate solution is obtained when using the crack distance given by the FIB Task Group 9.3 FRP (2001) or the Eurocode 2. However, the author suggests calculating the crack distance by using the FIB Task Group 9.3 FRP (2001) for those tests where no external load was applied before plate bonding.
6) Finally, a characteristic lower bound of the ratio V_{exp}/V_{pred} is obtained by the five-percentile as 0.87.
7) The verification of the proposal shows a better performance of the current model compared to the existing models when predicting peeling failure initiated near flexural or shear cracks.